

Summer 8-5-2019

Development of Experimental and Finite Element Models to Show Size Effects in the Forming of Thin Sheet Metals

Jeffrey D. Morris
University of New Orleans, jdmorris@uno.edu

Follow this and additional works at: <https://scholarworks.uno.edu/td>

Recommended Citation

Morris, Jeffrey D., "Development of Experimental and Finite Element Models to Show Size Effects in the Forming of Thin Sheet Metals" (2019). *University of New Orleans Theses and Dissertations*. 2676.
<https://scholarworks.uno.edu/td/2676>

This Thesis-Restricted is protected by copyright and/or related rights. It has been brought to you by ScholarWorks@UNO with permission from the rights-holder(s). You are free to use this Thesis-Restricted in any way that is permitted by the copyright and related rights legislation that applies to your use. For other uses you need to obtain permission from the rights-holder(s) directly, unless additional rights are indicated by a Creative Commons license in the record and/or on the work itself.

This Thesis-Restricted has been accepted for inclusion in University of New Orleans Theses and Dissertations by an authorized administrator of ScholarWorks@UNO. For more information, please contact scholarworks@uno.edu.

Development of Experimental and Finite Element Models to Show Size Effects in the Forming of
Thin Sheet Metals

A Thesis

Submitted to the Graduate Faculty of the
University of New Orleans
in partial fulfillment of the
requirements for the degree of

Master of Science
in
Engineering
Mechanical Engineering

by

Jeffrey D. Morris

B.S. University of New Orleans, 2014

August, 2019

Copyright 2019, Jeffrey D. Morris

Acknowledgement

I would like to thank Dr. Paul Schilling for his guidance and direction through each phase of the process that led to the production of this manuscript. I would also like to thank him for the opportunity to join the CIMM team; I would not have been able to seek a graduate degree without that support.

I would like to extend my thanks to Dr. Paul Herrington for serving as a committee member for my thesis defense. His suggestions and support were fundamental to improve the quality of this manuscript.

I would also like to extend my thanks to Dr. Uttam Chakravarty for serving as a committee member for my thesis defense. His suggestions and support were fundamental to improve the quality of this manuscript.

I would like to express my gratitude to my colleague Debabrata Mondal for his assistance in the computational modeling phase of this project. His efforts contributed significantly to the production of this manuscript.

This work was supported by the National Science Foundation through cooperative agreement OIA-15410795 and the Louisiana Board of Regents.

Table of Contents

List of Figures.....	v
List of Tables.....	vii
Nomenclature.....	viii
Abstract.....	ix
Chapter 1: Introduction.....	1
Chapter 2: Literature Review.....	2
2.1: Material Properties.....	2
2.2: Size Effects in Material Processes.....	3
2.3: Specimen Preparation and Testing of Materials.....	3
2.4: Forming Processes.....	4
2.5: Computational Modeling of Small-scale Size Effects.....	5
Chapter 3: Experimental Setup.....	6
3.1: Specimen Preparation.....	6
3.2: Tensile Testing and Material Characterization.....	7
3.3: Forming Experiment.....	9
3.4: Finite Element Modeling.....	10
3.5: Thickness Determination.....	11
Chapter 4: Results.....	12
4.1: Strain Gauge Test.....	12
4.2: Tensile Results.....	13
4.3: Experimental Forming Results.....	15
4.4: Simulation Forming Test Results.....	19
4.5: Cross-sectional Thickness.....	22
Chapter 5: Conclusions and Recommendations.....	25
5.1: Conclusions.....	25
5.2: Recommendations.....	25
References.....	27
Appendix.....	30
Vita.....	38

List of Figures

Figure 3.1.1: Images of the CNC machining process including: (a) Emco Concept Mill 55 machining a blank specimen, (b) machined blank and (c) tensile specimens, and geometric dimensions of the (d) tensile specimens and (e) blank specimens.....	7
Figure 3.2.1: UTS machine setup for a strain gauge test, showing Vishay P3 strain indicator.....	8
Figure 3.2.2: (a) UTS machine setup for a tensile test with (b) copper, (c) aluminum, and (d) resin, dog-bone tensile specimens.....	9
Figure 3.3.1: (a) UTS machine setup for a forming test with, (b) a close-up of the punch, die, and blank setup, and (c) copper and (d) aluminum, blank specimens.....	10
Figure 4.1.1: Load versus displacement results obtained from the strain gauge tests.....	12
Figure 4.2.1: Engineering stress versus engineering strain plots for 3d printed, resin dog-bone tensile specimens.....	13
Figure 4.2.2: Engineering stress versus engineering strain plots for aluminum 3003-H14 dog-bone tensile specimens of 0.8 mm, 0.6 mm, and 0.4 mm thicknesses.....	14
Figure 4.2.3: Engineering stress versus engineering strain plots for 99.9% copper dog-bone tensile specimens of 0.2 mm and 0.4 mm thicknesses.....	15
Figure 4.3.1: Punch load versus crosshead displacement plots for aluminum 3003-H14 blank specimens of 0.8 mm, 0.6 mm, and 0.4 mm thicknesses.....	16
Figure 4.3.2: Punch load versus crosshead displacement plots for 99.9% copper blank specimens of 0.4 mm and 0.2 mm.....	17
Figure 4.3.3: Final formed shapes of the die side for (a) 0.8 mm aluminum experiment, (b) 0.6 mm aluminum experiment, (c) 0.4 mm aluminum experiment, and the punch side for (d) 0.8 mm aluminum experiment, (e) 0.6 mm aluminum experiment, and (f) 0.4 mm aluminum experiment.....	18
Figure 4.3.4: Final formed shapes of the die side for (a) 0.4 mm copper experiment, (b) 0.2 mm copper experiment, and the punch side for (c) 0.4 mm copper, and (d) 0.2 mm copper experiments.....	18
Figure 4.4.1: Comparison of experimental and numerical plots of punch load versus crosshead displacement results obtained for aluminum 3003-H14 blank specimens of 0.8 mm, 0.6 mm, and 0.4 mm.....	19
Figure 4.4.2: Comparison of experimental and numerical plots of punch load versus crosshead displacement results obtained for 99.9% copper blank specimens of 0.4 mm and 0.2 mm.....	20

Figure 4.4.3: Final formed shapes of (a) 0.8 mm aluminum experiment, (b) 0.6 mm aluminum experiment, (c) 0.4 mm aluminum experiment, (d) 0.8 mm aluminum simulation, (e) 0.6 mm aluminum simulation, (f) 0.4 mm aluminum simulation, (g) 0.2 mm copper experiment, (h) 0.4 mm copper experiment, (i) 0.2 mm copper simulation, and (j) 0.4 mm copper simulation	21
Figure 4.5.1: Comparison of normalized thickness versus final radius plots for the 0.4 mm copper experiment, the 0.2 mm copper simulation, and 0.4 mm copper simulation.....	22
Figure 4.5.2: Cross sectional wedges displaying the thickness through the (a) 0.2 mm and (b) 0.4 mm simulated copper forms.....	23
Figure 4.5.3: Cross-sectional macrographs of the 0.4 mm copper formed specimen, (a) as a series of the entire cross-section pieced together from twelve images to measure the final radius, and (b) and individual macrograph, displaying the method used to measure the thickness.....	24
Figure A.1: Diagram showing a wire-cutting EDM process.....	30
Figure A.2: MK diamond wet saw, and sectioning setup.....	30
Figure A.3: Images of: (a) the end-mill mounted in the collet, and (b) the CNC machining setup.....	31
Figure A.4: SolidWorks model of the hemispherical (a) punch and (b) die.....	31
Figure A.5: 3d-printing setup for the hemispherical punch and die in PreForm slicer software.....	32
Figure A.6: Images of simulation assembly (a) symmetry conditions and (b) mesh for 0.4 mm copper.....	33
Figure A.7: Contours of (a) Von Mises stresses, and (b) equivalent plastic strain, for the 0.8 mm aluminum forming simulation.....	34
Figure A.8: Contours of (a) Von Mises stresses, and (b) equivalent plastic strain, for the 0.6 mm aluminum forming simulation.....	34
Figure A.9: Contours of (a) Von Mises stresses, and (b) equivalent plastic strain, for the 0.4 mm aluminum forming simulation.....	34
Figure A.10: Contours of (a) Von Mises stresses, and (b) equivalent plastic strain, for the 0.4 mm copper forming simulation.....	35
Figure A.11: Contours of (a) Von Mises stresses, and (b) equivalent plastic strain, for the 0.2 mm copper forming simulation.....	35
Figure A.12: Composite image of copper 0.4 mm cross sectional macrographs, showing the method of determining the final formed radius measurements.....	36
Figure A.13: Macrographs of various cross-sections showing the method of thickness measurement (a) 4.78 mm (b) 4.50 mm (c) 4.06 mm (d) 3.50 mm (e) 2.69 mm (f) 1.59 mm.....	37

List of Tables

Table 3.1.1: Processing parameters used to machine the tensile and blank specimens, for both aluminum and copper	6
Table 3.3.1.: 3d print and post processing settings used to fabricate the punch and die.....	9
Table 3.4.1: Material properties used in ABAQUS for each material.....	11
Table 4.1.1: Load versus displacement results from the strain gauge test.....	13
Table 4.5.1: Results of normalized thickness vs final radius plots for the 0.4 mm copper experiment, the 0.2 mm copper simulation, and 0.4 mm copper simulation.....	23
Table A.1: Strain gauge specifications, testing parameters, and tensile specimen dimensions.....	31
Table A.2: Tensile properties of aluminum 3003-H14 for varying ranges of sheet thickness [33].....	32
Table A.3: Tensile properties of 99.9% copper [34].....	32
Table A.4: Measured cross-sectional geometry (thickness and width) of the dog-bone tensile specimens, for each material.....	33
Table A.5: Plastic flow inputs for the aluminum and copper simulations.....	33

Nomenclature

σ	stress
σ_e	engineering stress
σ_t	true stress
σ_y	yield stress
σ_o	frictional stress (material constant)
ϵ_e	engineering strain
ϵ_t	true strain
ϵ_p	plastic strain
ϵ_y	yield strain
ϵ_f	excessive values of strain
k_y	strengthening coefficient (material constant)
F	force
A_o	initial cross-sectional area
L_o	initial length
ΔL	change in length
E	elastic modulus
n	strain hardening exponent
S	sheet thickness of final form
S_i	initial sheet thickness
r_i	initial radius
r_f	radial distance of final form
ω	spindle speed
v_{cs}	cutting speed
D_t	tool diameter
t	thickness of specimen
w	width of specimen
d_g	average grain diameter

Abstract

An experimental method was developed that demonstrated the size effects in forming thin sheet metals, and a finite element model was developed to predict the effects demonstrated by the experiment. A universal testing machine (UTM) was used to form aluminum and copper of varying thicknesses (less than 1mm) into a hemispherical dome. A stereolithography additive manufacturing technology was used to fabricate the punch and die from a UV curing resin. There was agreement between the experimental and numerical models. The results showed that geometric size effects were significant for both materials, and these effects increased as the thickness of the sheets decreased. The demonstration presents an inexpensive method of testing small-scale size effects in forming processes, which can be altered easily to produce different shapes and clearances.

Keywords: stereolithography punch/die; geometric size effects; hemispherical cup-forming experiment; aluminum and copper; finite element model

Chapter 1: Introduction

There are multiple length and time scales that must be considered for prediction of physical phenomena; these scales are often generalized as: macro-, meso-, micro-, and atomistic scales. Classical physics models are used to make predictions from the macro scale to the upper end of the atomistic scale, depending on the specifications of the problem; these theoretical models consider time and space to be a continuum. The computational methods of prediction that are based on continuum mechanics, often lose predictive power in the micro/meso range of the scale due to size effects. Some methods of offsetting these errors involve incorporating numerical models that are used to make predictions at varying ranges of the scale spectrum [1].

Another issue that arises, involves obtaining accurate results from experimental testing at small scales. The size of the specimen geometry requires that specific preparation techniques must be employed to avoid errors that produce inconsistent, and inaccurate results. Errors in testing results can result from a variety of phases of an experiment, including: specimen preparation, accuracy of testing machinery, accuracy of measurements, and post-processing/analysis of data. The consequences of poor testing techniques can cause the loss of time and money, and lead to conclusions that are unreliable.

In this study, an experiment that demonstrated the size effects in thin sheets of aluminum and copper that arise in forming processes was developed. A UTM was used to form aluminum 3003-H14 sheet thicknesses of 0.8 mm, 0.6 mm, and 0.4 mm, and 99.9 % copper sheet thicknesses of 0.4 mm and 0.2 mm, into hemispherical dome shapes. The results of these tests were then compared to the results of a finite element (FE) simulation, which was developed using ABAQUS.

Important aspects of the experiment included: the design and fabrication of the punch and die using an additive manufacturing technique, the preparation of dog-bone tensile specimens and forming blank specimens using a computer numerically controlled (CNC) process, the conduction and data processing of tensile and forming tests, and post-processing of the formed specimens. The results of the tensile tests were used as inputs for the FE model to characterize the elastic behavior of the punch and die, and the severe plastic deformation response of the thin metal forms.

The results of the experiment showed good agreement with the numerical simulation, and the expected results. The final geometry of the experimental and numerically simulated forms showed a crinkle pattern around the brim of the hemispherical domes. The number of crinkles and symmetry of the crinkle pattern were not identical for each thickness and material, but the trend of increased frequency of crinkles at smaller thicknesses was demonstrated. There was also good agreement between the outputs of punch load versus crosshead displacement for all thicknesses of each material.

There were several errors that most likely caused some of the inconsistencies in the final results of the experiment. The specimen preparation technique could be improved upon, or changed entirely. The FE model could also be improved to include anisotropy.

Chapter 2: Literature Review

This chapter contains: the equations that were relevant to the experiment, a brief description of the size effects associated with small scale processes, and referenced literature of similar setups, which involved specimen preparation, tensile testing, forming, and computational models.

2.1 Material Properties:

The data collected from the UTS includes engineering stress and engineering strain; the equations for engineering stress and engineering strain are [2],

$$\sigma_e = F/A_0$$

$$\varepsilon_e = \Delta L/L_0$$

The stress versus strain plot includes elastic and plastic regions. The plastic region of the stress strain curve is characterized by significant deformation which changes the cross-sectional area of the specimen, therefore the stress versus strain curve must be adapted to reflect this. Engineering stress and engineering strain are converted to true stress and true strain as shown [2],

$$\sigma_t = \sigma_e(1 + \varepsilon_e)$$

$$\varepsilon_t = \ln(1 + \varepsilon_e)$$

Severe plastic deformation is characteristic of forming processes. A modified version of the Ramberg-Osgood equation is used to characterize the effect of strain hardening in materials at large deflections. The results from tensile tests are used as inputs to determine a stress versus strain curve and a strain hardening exponent; these results are then used as inputs to an FE model to calculate plastic deformation.

$$\varepsilon_f = \sigma/E + 0.002(\sigma/\sigma_y)^{1/n}$$

The Hall-Petch equation estimates the change in yield strength with respect to grain size for a particular material. While this equation does not consider the grain size effects that are present at small scales, it is still used in models as a scaling parameter to make a revised estimate. The Hall-Petch equation is [2]:

$$\sigma_y = \sigma_o + \frac{k_y}{\sqrt{d_g}}$$

2.2: Size Effects in Material Processes

Two types of size effects that lead to inaccurate predictions have been demonstrated in material processes in the meso/microscale range of theoretical and computational models; they are geometric size effects and grain size effects. Geometric size effects occur when the ratio of the workpiece dimensions to the testing dimensions reach a critical point for the material, and testing specifications. This type of size effect can result in a final geometry or material properties that were not expected, or desired. Grain size effects occur in conjunction with geometric size effects, and cause the material properties of a specimen to change significantly, for equal geometries.

2.3: Specimen Preparation and Testing of Materials

Testing materials in the small-scale range of the spectrum presents difficulties due to the accuracy that must be achieved with respect to tolerances, optimization of surface finish, and machine compliance. Huerta, et al. [3] described a method for determining machine compliance of a miniature UTM, which involved attaching a strain gauge to a tensile specimen and calculating a spring constant for the machine.

Proper parameter determination is of critical importance to achieving the desired surface finish in machining processes. The cutting speed must first be determined for the specific workpiece material, tool geometry, and tool material. Appropriate tables and calculations are referenced in determination of cutting speed, feed rates, and spindle speed [4]; this equation is shown as,

$$\omega = (v_{cs} * 12) / (\pi * D_t)$$

Much experimental research has been conducted on tensile specimens of varying scales, to demonstrate the size effects associated with small scale specimens. Gong et al. [5] performed tensile tests on thin copper sheets ranging from thicknesses of 40-320 microns, at varying gage lengths, and showed that the flow stress and elongation decreased as the thickness decreased. Similar behavior was demonstrated in carbon steel at thicknesses of 50-100 microns [6], and similar thickness brass sheets [7].

Several methods of small-scale specimen preparation have been developed to optimize the surface finish in metals. Electric discharge wire cutting is a widely used technique of producing small scale testing specimens [8]. This process uses the sparks between an electrode and a workpiece that is electrically conductive to erode the material, and clears the residue with a dielectric fluid [9]; a diagram of wire-cutting EDM is shown in the appendix in figure A.1. Micro-end milling is a process that considers the minimum chip thickness, grain size effect, and micro-burr formation [10]. This process varies significantly from traditional macro milling processes.

Physical vapor deposition (PVD) is a technique used in nanomaterial fabrication, to produce thin films and coatings. One method of PVD entails using a sputter gun in a vacuum, to transition material particles from a condensed phase to a vapor phase, and then re-condensing the material particles onto a substrate material; this is followed by a thermal treatment to achieve material consolidation [11]. Vapor deposition has been used to produce sub-micro test specimens for testing of thin films, which are used to coat machine parts and tools [12].

The parameters used in the post-processing step of curing the 3d printed resin punch and die, have a significant effect on the final material properties. Zguris [13] showed that the tensile strength of Formlabs resin increased with curing temperature, up to 60 °C. The tensile strength also increased steadily through the first 30 minutes of the curing process, and then showed only a gradual increase through the next 15-30 minutes.

2.4: Forming Processes

There are a variety of forming processes used to shape materials, or enhance the physical properties of a material; these methods include the various techniques of: shearing, bending, drawing, extrusion, rolling, forging, and bulge forming [14]. Important considerations in all forming processes are the material properties, such as plasticity and anisotropy, and the process variables of friction and lubrication [15]. These manufacturing processes have become more prevalent at smaller scales, due to the broad application in advancing technologies, such as micro-electro mechanical systems (MEMS) [16].

Raulea, et al [17] demonstrated that the yield strength of soft aluminum sheets decreased as the number of grains across the sheet thickness decreased, in a planar blanking process. Chan, et al. [18] showed that deformation load, interfacial friction, and microstructural evolution contribute to inhomogenous deformation in multiple extrusion processes. Kumar, et al. [19] used a theoretical model to predict the final thickness geometry through the cross-section of an AL 7475 hemispherical dome, which was formed by a superplastic bulge forming process. Analytical and FE models have been used in conjunction to evaluate side wall crinkling in sheet metal forming processes [20].

Forming processes require lubrication to reduce the friction at surface interfaces, which creates issues in the evaluation of the coefficient of friction (CoF). Various theoretical, experimental, and computational methods are used to evaluate the effect of friction in forming processes. The CoF for a specific surface interaction is often categorized along a spectrum as: dry, boundary lubrication, mixed-layer lubrication, or hydrodynamic lubrication [21]. Olsson, et al. [22] developed a tribological test to measure the effectiveness of lubrication in deep drawing processes, by measuring the maximum backstroke force on the punch. Finite element analysis have been developed to predict the CoF in AL 1100 for the purpose of advancing design in workpieces and tooling in forming processes [23].

Cao, et al. [24] used a UTM loading stage to produce micro-extrusion of brass and steel alloys. The compression platens were replaced by a ram/die assembly, which was machined using the previously described EDM technology. Micro-pins of 1.0 mm diameter were extruded from heat treated specimens, which had a wide range of grain size.

Micro-forming processes are a subset of micro-manufacturing, which involves developing technology that achieves greater throughput volume of micro-parts than conventional manufacturing processes, by using a smaller system known as a micro-factory [25]. The EU MASMICRO project developed the manufacturing execution system (MES), which includes micro-milling, micro-hydro-forming, and micro-bulk-forming machines [26]. The purpose of this four year (2004-2008) project was to develop mass production processes, miniature bench-top equipment, and ultra-precision techniques, in micro-manufacturing.

2.5: Computational Modeling of Small-scale Size Effects

Several methods of modeling the size effects in forming processes have showed agreement with experimental results. Some of these methods include modeling a generalization of the grain structure, effective treating the material as having composite properties, rather than bulk material properties.

Liu, et al. [27] proposed a constitutive model, in which the surface layer grain structure was treated differently than the inner grain structure. The inner grains were treated as a composite of grain interior and a work-hardened grain boundary, and the surface was modeled with no grain boundaries. Other models have employed a Voronoi tessellation algorithm, which generates a grain structure with a particular grain size. The various grains are then assigned varying material properties, which were determined from the bulk material properties [28]. Engel, et al. [29] have developed two approaches to modelling material flow and friction in micro-forming. The first model was a mesoscopic model, in which a synthetic grain structure (similar to a Voronoi tessellation) was generated and the surface layer and inner layers were given separate properties [30]. The second model was a combination of the general friction law and mechanical rheological model, which characterized the surface topography as having sections of different roughness [29]. Sanusi, et al. [31] developed a finite element model that predicted the deformation in nanocrystalline metals which had been subjected to an equal channel angular press forming process; this model considers both grain size and grain misorientation, and can be used to re-mesh the grains that experienced severe plastic deformation.

Several models incorporate the Hall-Petch equation, which relates the yield strength of a metal to grain size. Ni, et al. [32] investigated the geometric size effects in copper and aluminum, and developed a scaling model that combines both geometric and grain size effects; this scaling parameter was then introduced into the Hall-Petch equation.

Chapter 3: Experimental Setup

An experiment was developed to demonstrate the geometric size effects that are present in the forming of thin sheet metals (less than 1 mm in thickness). The experiment was designed to form aluminum and copper circular blanks of varying thicknesses, into hemispherical dome shaped bowls. The methodologies of: specimen preparation, material characterization, forming process setup, simulation model setup, and final form cross-sectional thickness determination are presented in the following sections of this chapter.

3.1: Specimen Preparation

Tensile and blank specimens were prepared using a computer numerically controlled (CNC) machining process. The Emco Concept Mill 55 was used to create dog-bone tensile and three forming blank specimens for all sheet thicknesses of both metals. Sheets of aluminum 4" x 12" were sectioned into 2" x 4" sheets using an MK Diamond-370 EXP wet saw. A corrugated paper sheet was placed on the cutting bed to protect the metal workpiece surface from being scratched; this setup is shown in figure A.2. The edges of the 2" x 4" sheets were then filed with a razor to remove all of the burs and flashing, so that a flat sheet remained. The flat sheets were bonded to a sacrificial wooden block using cyanoacrylate, to ensure a rigid workpiece for the machining process; this was necessary to achieve an optimal specimen surface finish. A standard size 2 x 4 was cut into 5" segments, leaving a working surface that was approximately 5" x 3.5"; these dimensions were used to ensure the entire surface area of the metal sheets would sit on the wood, with no overhangs. The metal sheets were centered on the wooden block, and the outline was marked. The surface of the wood was then lightly moistened with water, and a thin layer of cyanoacrylate was spread within the marked borders. The metal sheets were then placed on the bed of glue and floated back and forth to ensure there was complete coverage, and the workpiece was well bonded to the wooden block; the finished workpiece was left for 24 hours to allow the bond to adequately cure. Images of the end-mill and CNC machining setup are shown in figure A.3.

The WinCam CNC software was opened, and the geometry of the specimens and workpiece were input in the CAD section. The CAM section was accessed, and the machining parameters were entered to program the G-code. The workpiece was placed into the vise of the machine, and the NC section was opened. The edges of the workpiece and vise were input by moving the tool to a reference point, and marking each edge. The program cycle was started, and the process was observed to ensure proper machining. After the machining was completed, the workpiece was removed from the vise, and the surface was inspected. The workpiece was placed into an acetone bath to dissolve the bond, and all remaining residue was removed from the specimens. The prepared specimens were observed with at 10x magnification to confirm an adequate surface finish. The parameters used to machine the specimens are shown in table 3.1.1, and images of the equipment, workpieces, and the dimensions of the metal specimens are shown in figure 3.1.1.

Table 3.1.1: Processing parameters used to machine the tensile and blank specimens, for both aluminum and copper

Tool Diameter	Number of Flutes	Feed Rate	Spindle Rate	Cutting depth
6 mm	4	4 IPM	1700 rpm	0.12 in

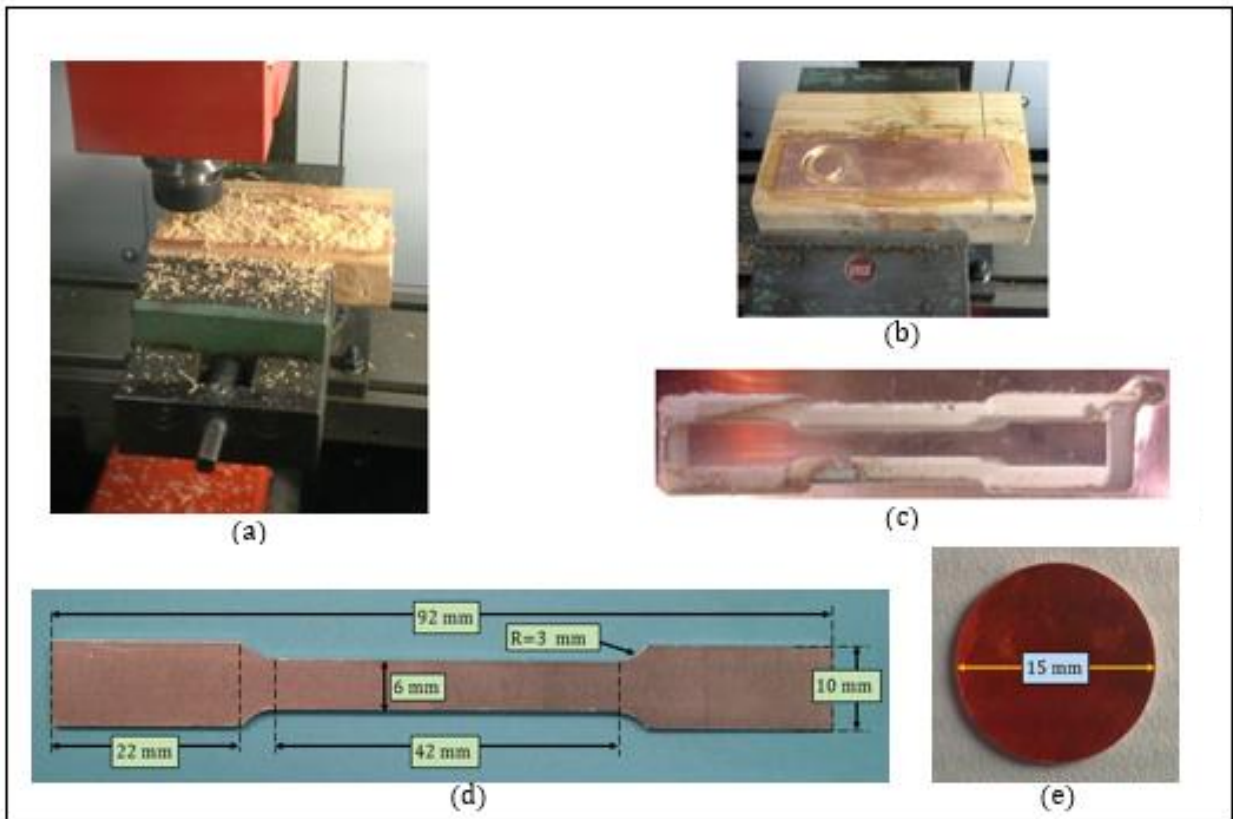


Figure 3.1.1: Images of the specimen preparation process, including: (a) Emco Concept Mill 55 machining of a blank specimen, (b) copper machined blank and (c) tensile specimens, and geometric dimensions of the (d) tensile specimens and (e) blank specimens

3.2: Tensile Testing and Material Characterization

The dog-bone specimens were tested on a miniature UTM to obtain the plot of flow stress versus strain, which was later used in the FE model. The accuracy of the machine was assessed by installing a Micro Measurements strain gauge in a quarter-bridge configuration, to an aluminum tensile specimen, and then comparing the results from the strain indicator to the outputs from the UTM. The TestWorks 4 UTM software was opened, and a tension test was selected from the menu. The tensile specimen was placed on top of the grips, and the crosshead was adjusted to an adequate separation distance between the grips. The distance between the grips was measured with Neiko calipers, and entered into the software. The grips were then tightened to hold the specimen loosely, so that no load was measured on the specimen. The strain gauge was then connected to the Vishay P3 strain indicator, and set to measure displacement in millimeters. The strain gauge was calibrated and balanced, so that a zero displacement was indicated. The grips were then tightened so that the specimen was adequately secured; the load that was indicated in TestWorks 4 was observed throughout this process, and an attempt was made to minimize the load on the specimen. The testing parameters and specimen dimensions were entered into the software, and the test was started; the

crosshead velocity was set as 0.3 mm/min. The test was paused at varying points within the elastic deformation range of the specimen, and to record the measured load and displacement from the software, and the displacement from the strain indicator. The strain gauge setup is shown in figure 3.2.1, and the input parameters are shown in table A.1.

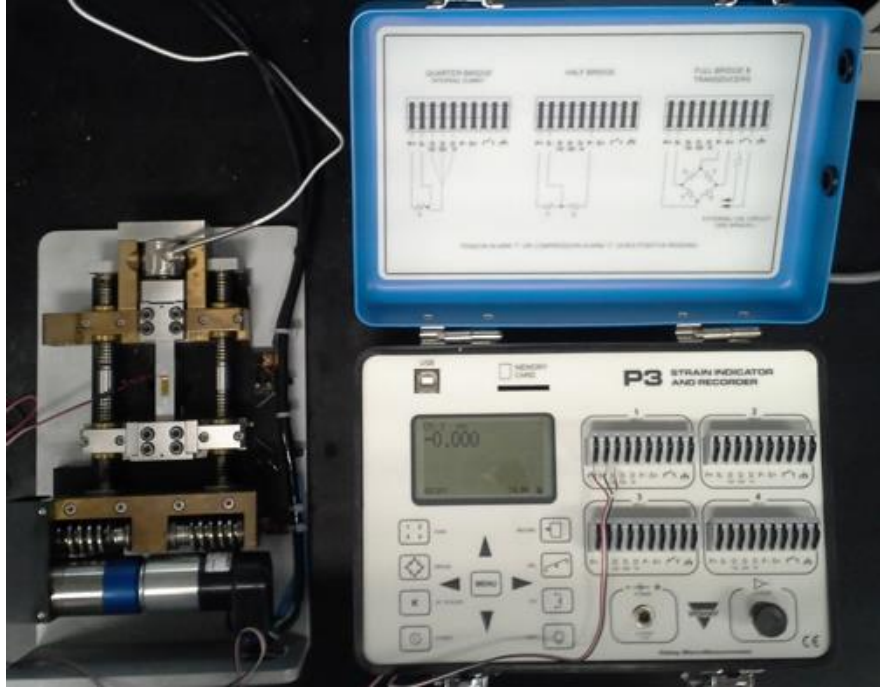


Figure 3.2.1: UTS machine setup for a strain gauge test, displaying Vishay P3 strain indicator

The TestWorks 4 software was then used to conduct the tensile tests for each specimen material and thickness. The software was opened, and the test was set up using the procedure described above (with the strain gauge omitted); the sample rate was set to 2.0 Hz, and the crosshead velocity was set to 0.5 mm/min. The cross-sectional dimensions of each specimen were measured at several points along the gage length, using a Mitutoyo micrometer. The measurements of width and thickness were recorded, and these values are shown for each material in table A.4. The test was started and allowed to run until the specimen fractured. The specimen was removed from the grips, and the data was downloaded. The tensile stage setup and images of the copper, aluminum, and the resin dog-bone specimens are shown in figure 3.2.2; the dimensions of the resin specimens differed from the metal specimens; these dimensions are included in figure 3.2.2.

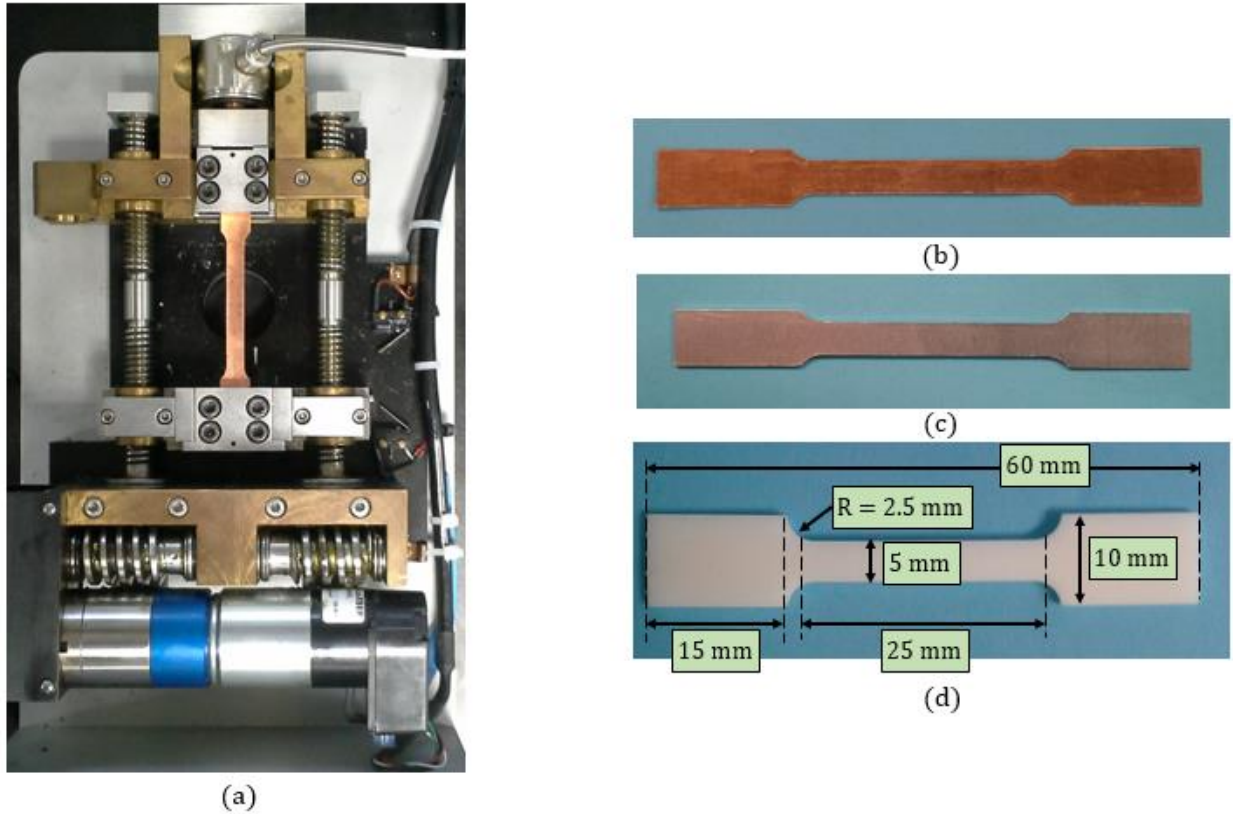


Figure 3.2.2: (a) UTS machine setup for a tensile test with (b) copper, (c) aluminum, and (d) resin, dog-bone tensile specimens

3.3: Forming Experiment

A miniature UTM was used to form circular blanks of each metal at varying thicknesses into a hemispherical dome-shape. The Formlabs Form 2, which employs stereolithography additive manufacturing technology, was used to fabricate the punch and die with Formlabs resin. The compression platens were removed from the machine, and the dimensions were measured with calipers. These measurements were then used to design the compression platens in SolidWorks, and the punch and die were modeled into the testing face of the platens; images of the punch and die models are shown in figure A.4. This SolidWorks file was converted into an STL, and imported into PreForm software to set the orientation and parameters for the print. The parts were oriented so that the punch and die faced in the vertical direction during printing to avoid having supports placed on them; figure A.5 shows an image of the PreForm setup. The finished prints were removed from the build platform and washed in an isopropyl alcohol bath for 20 minutes. The Form Cure was then used to cure the parts, and the supports were removed with shears; the print settings and curing parameters are shown in table 3.3.1.

Table 3.3.1: 3d print and post processing settings used to fabricate the punch and die.

Material	Layer Thickness	Print Time	Wash Time	Cure Time	Cure Temp
White V4 Resin	0.025 mm	3 h 45 min	20 min	45 min	60 °C

The TestWorks 4 software was opened, and a compression test was selected. The platens were removed and replaced with the punch/die, and the alignment and clearance was checked. This was accomplished by setting a sheet of metal of known thickness on the die, and moving the crosshead until a force was recorded; the sheet was then removed, and the crosshead was moved farther toward the punch until a force was again observed. There were no forces observed on the test until the punch was located approximately 4.9 mm below the top the die cavity.

To setup the test, the punch and die were separated by an adequate distance (approximately 15 mm) so that each side of the die could be accessed adequately. Silicon lubrication was applied to the interacting surfaces of the punch, die, and blank, to reduce the CoF for the test. The circular blank specimen was then placed on the die, and a 10x magnifier was used to confirm proper alignment by measuring the distance from the edges of the specimen nearest to each edge of the die. The crosshead was then slowly displaced until a slight force (under 5.0 N) was observed, and then backed away until the force was removed; the force and crosshead displacement were zeroed, and the test parameters were entered. The test was started, and allowed to run until a displacement of 5.0 mm was reached, at which point the test was manually stopped. Testing data was exported, and the specimen was removed from the machine. The UTM setup and forming specimens are shown in figure 3.3.1.

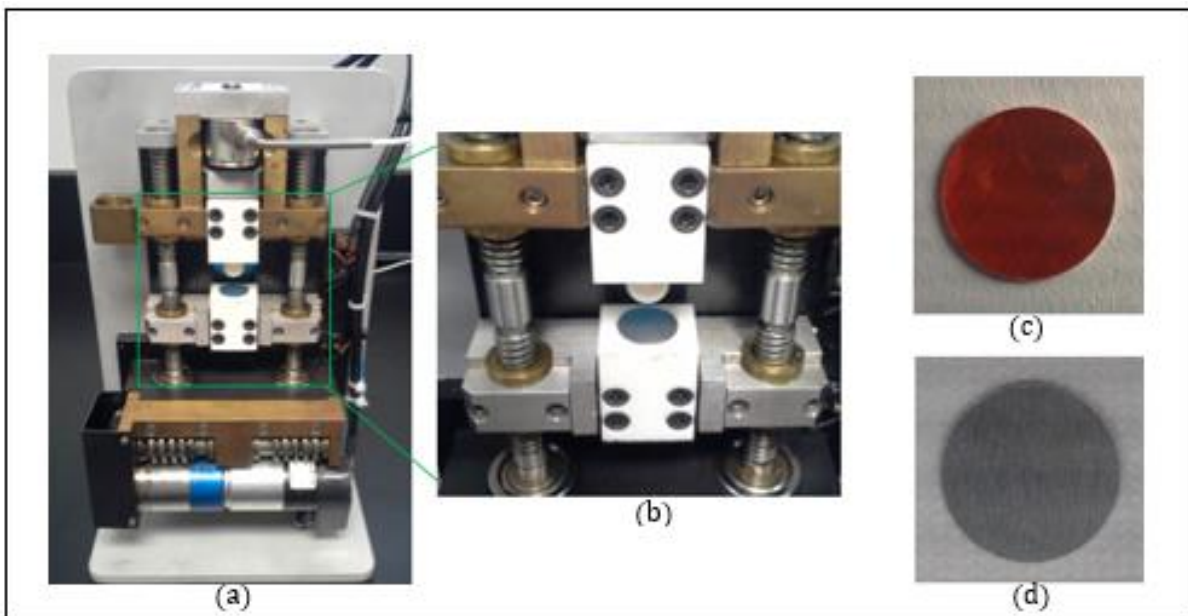


Figure 3.3.1: (a) UTS machine setup for a forming test, with (b) a close-up of the punch, die, and blank setup, and (c) copper and (d) aluminum blank specimens

3.4: Finite Element Modeling

An FE model was developed in ABAQUS to compare the load versus displacement data with the experimental results, and to compare the cross-sectional thickness variation to the expected theoretical value.

The form test system dimensions were designed in the PART window by entering the profile dimensions of the punch, die, and workpiece in the XY-plane, and extruding this profile one-quarter

revolution around the Y axis. The material properties were entered into the PROPERTY window; the tensile tests were used in conjunction with the Ramberg-Osgood equation to determine the properties of both materials. The tensile properties of each material are shown in table 3.4.1, and the plastic flow stress input values are shown in table A.5. Two instances were created for the punch/die and blank in the ASSEMBLY window, and each part was translated to replicate the initial positions in the experimental setup. The interacting surfaces were then assigned in the PART window, and a friction factor of 0.04 was assigned to these surfaces in the INTERACTION window. The boundary conditions for the form system were assigned in the LOAD window. A fixed boundary condition was assigned to the bottom of the die, and symmetry boundary conditions were assigned to each edge surface on the XY and ZY axes. The top of the punch was assigned a displacement condition to translate the punch 5.0 mm in the Y direction. Each part was meshed in the MESH window separately; the punch was meshed with TET elements, whereas the die and workpiece were meshed with HEX elements. The desired outputs of punch displacement and reaction force at the top of the punch were assigned in the JOB window by creating a history output request. The model was saved, and then assigned to run in the JOB window, which took approximately 45-120 minutes, depending on the final mesh and specimen size. Images of the assemble symmetry conditions and mesh are shown in figure A.6.

Table 3.4.1: Material properties used in ABAQUS for each material

Material	Modulus of Elasticity (GPa)	Yield Stress (MPa)	Ultimate Stress (MPa)
Aluminum	69	115	160
Copper	110	90	171
Resin	2.4	NA	NA

After the simulation was completed, the output database (ODB) history was opened. The formed workpiece was mirrored along the XY and YZ symmetry planes to show a full-sized blank. The Mises stress and plastic equivalent strain contours were applied, and images of these were captured. The reaction force at the top of the punch was then plotted as a function of punch displacement. The cross-sectional specimen thickness was measured at various nodes by accessing the QUERY window, and using the DISTANCE tool.

3.5: Thickness Determination of the Experimental Formed Specimens

To determine the thickness distribution of the hemispheres, the specimens were mounted using a resin epoxy, and allowed to cure for 48 hours. The Allied Techcut 4 was then used to cut the mounted forms to expose the cross-sectional thickness of the specimen. The cut specimens were cleaned in an isopropyl alcohol bath, and the Olympus GX microscope was then used to capture images a 5x magnification. These images were imported into PowerPoint, and a line was drawn over the 200 micron scale bar as a reference measurement; the length of this line was obtained from the Format Shape/Size window. Another line was drawn tangent to the convex surface of the formed specimen, and a final line was drawn through the thickness of the specimen, which was perpendicular to the tangent line. This process was repeated at seven points along the cross-section, which was determined by taking the top of the odd-numbered macrographs for reference purposes. All of the images were then incorporated into a single image that shows the entire cross-section and thickness distribution.

Chapter 4: Results

The results of the strain gauge test, tensile tests, forming experiments, and computational models are presented in this chapter. The strain gage results were used to confirm the accuracy of the UTS. The tensile tests results were used as inputs into the Ramberg-Osgood model, and these results were used as inputs into the computational model to obtain the plastic flow stress versus plastic strain plot. Load versus displacement plots for the forming experiments and simulations are compared for each material at varying thicknesses; the experimental results are then compared to the simulation results for each material. Images of the final form shapes are shown for both the experiments and the simulations; the crinkle pattern from the experimental results were compared for the varying thicknesses, and then compared with the simulation results for similar thicknesses. The cross-sectional thickness of the final formed shape was obtained for the simulation, and the thickness was plotted as a function of radial distance. These plots were compared with measurements of the final form thickness of the experimental specimen, which were obtained by cutting the form to expose the radial cross-section, and magnifying the specimen.

4.1: Strain Gauge Test

The load versus displacement plots for the UTM and strain gauge are shown in figure 4.1.1, and the values are shown in table 4.1.1. The test showed that the slope of the strain gauge and total loads were 4.3 kN/mm and 4.8 kN/mm, respectively. The results from the UTM show that the initial 50 microns of crosshead displacement did not match the rest of the slope. This was most likely caused by bending initial bending stresses outside of the uniaxial direction that were applied to the specimen as the grips were tightened. As the uniaxial tension set in, these conditions were overcome, and became negligible; this issue presents no effect in the forming experiment, because there is no preload condition caused by the grips. Residual stresses from the machining process may have also contributed to this condition of slipping at the start of the test.

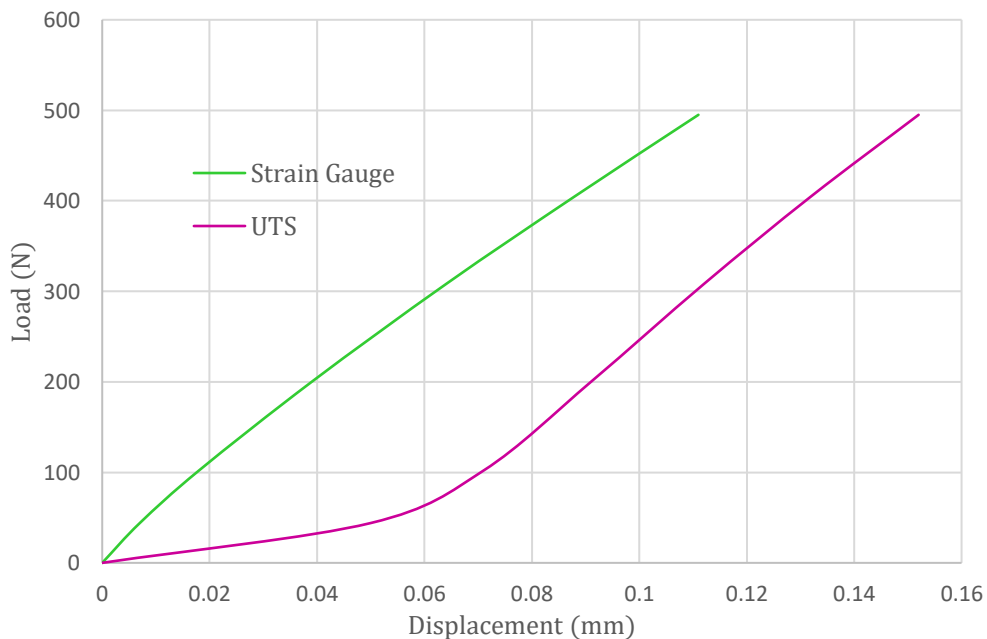


Figure 4.1.1: Load versus displacement results obtained from the strain gauge tests

Table 4.1.1: Load versus displacement results from the strain gauge test

Strain gauge Displacement (mm)	Crosshead Displacement (mm)	UTM Measured Load (N)
0	0	0
0.007	0.050	44.3
0.018	0.071	102
0.039	0.091	200
0.064	0.112	308
0.088	0.132	405
0.111	0.152	495

4.2: Tensile Results

The results from the tensile tests for the 3d-resin, and each thickness of aluminum and copper are presented in this section. The results for the metal specimens followed the expected effect of geometric size, in that the yield stress and elongation decreased with decreasing sheet thicknesses.

The results of the tensile tests for the 3d printed resin are shown in figure 4.2.1. The results show that the resin is a brittle material, and plastic deformation would not be expected. The modulus and yield strength were approximated to be 2.40 GPa and 53 MPa, respectively.

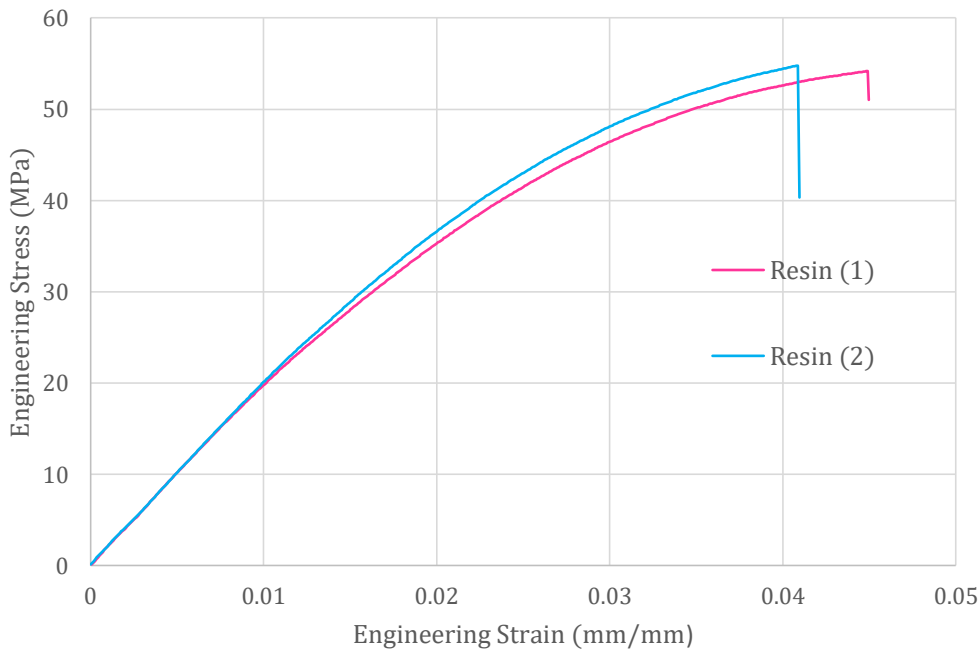


Figure 4.2.1: Engineering stress versus engineering strain plots for 3d printed, resin dog-bone tensile specimens

The stress versus strain plots from the aluminum tensile tests for three sheet thicknesses are shown in figure 4.2.2; there are some inconsistencies in these tests that were most likely due to issues with specimen preparation. Several specimens using the geometry used for the resin samples were initially prepared, and tested. The geometry of these specimens did not adhere to ASTM standards, so specimens were prepared using the 0.8 mm and 0.6 mm thickness sheets.

The moduli of all specimens were consistent, though the magnitude was significantly less than the moduli for Al 3003-H14 that was obtained from literature. The yield and ultimate strengths of the 0.8 mm and 0.6 mm specimens showed good agreements with expectations, in that there was a slight decrease in each property as the thickness decreased. The 0.4 mm specimens exhibited some irregular behavior; the yield was more gradual, and occurred at a lower magnitude, and the ultimate strength occurred with minimal extension.

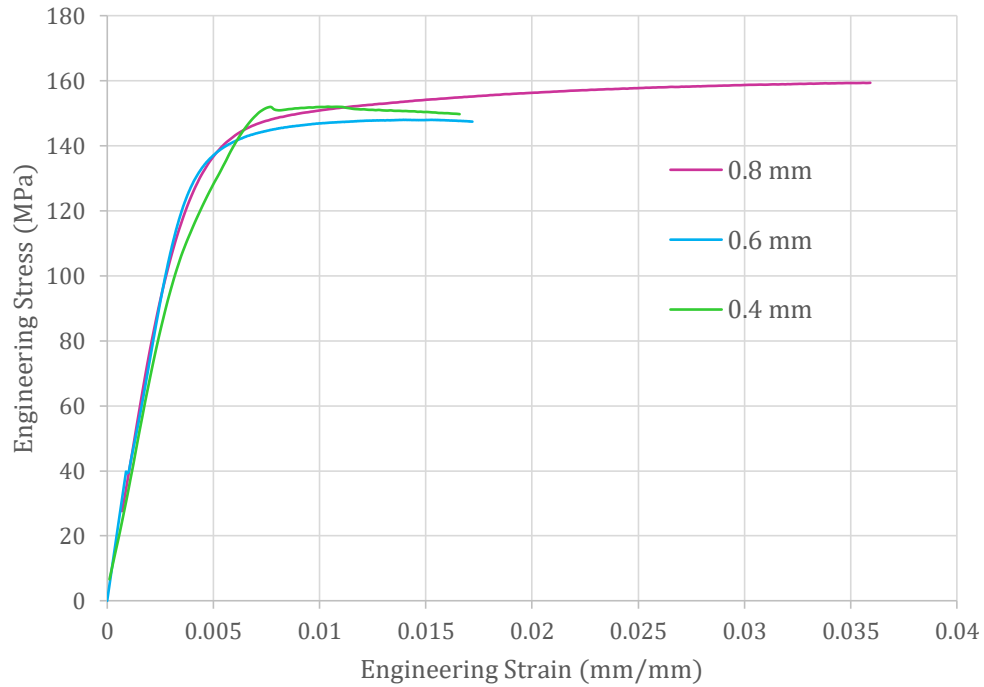


Figure 4.2.2: Engineering stress versus engineering strain plots for aluminum 3003-H14 dog-bone tensile specimens of 0.8 mm, 0.6 mm, and 0.4 mm thicknesses

Plots of the tensile results for the copper specimens of each thickness are shown in figure 4.2.3. The results from these tests were more consistent with expectations than those for the aluminum. The yield strength was determined by drawing a line 0.2 % offset from the modulus. The modulus and yield strengths for each thickness were approximately the same values. The ultimate strength and elongation were greater for the 0.4 mm specimen, which was expected.

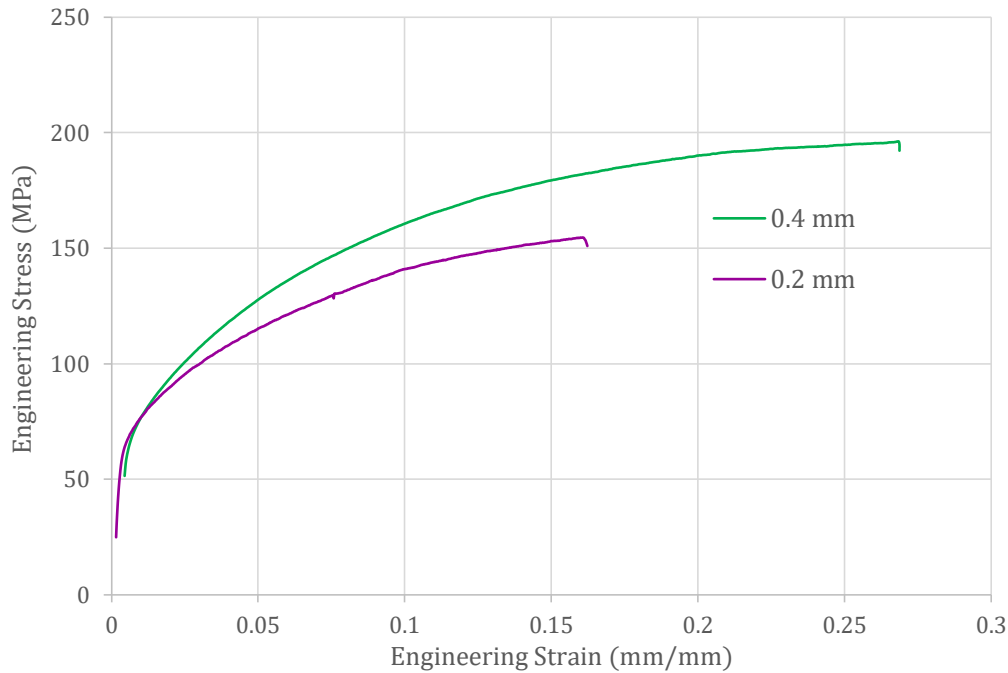


Figure 4.2.3: Engineering stress versus engineering strain plots for 99.9% copper dog-bone tensile specimens of 0.2 mm and 0.4 mm thicknesses

4.3 Experimental Forming Results

In this section the load versus displacement plots from the aluminum and copper forming tests are presented and explained. Pictures of the final formed shapes of all specimens are presented, which show the effects that initial sheet thickness had on the final geometry of the specimens.

The load versus displacement plots for two specimens of each thickness are shown in figure 4.3.1. There was a significant degree of consistency in the results for all thicknesses. The plots show some expected trends were consistent with size effects. There are two distinct regions of the plots for all of the tests. The first portion of the plot was primarily a result of bending in the specimens, which occurred from the start of the test until approximately 3.4 mm, 3.6 mm, and 3.8 mm for the 0.8 mm, 0.6 mm, and 0.4 mm thicknesses, respectively. The second portion of the plot was characterized by an increased load versus displacement slope, which was caused by a transition from bending, to a tensile membrane response. As the displacement reaches the length of the punch/die radius, there were increased points of contact between the blank and the punch/die, and the specimen starts to form around the punch and stretch. There was a more obvious change in slope in the 0.4 mm specimen at approximately 3.8 mm of displacement. The transition in slope became less obvious as the specimen thickness increased, and the 0.8 mm plots resemble a smooth exponential curve.

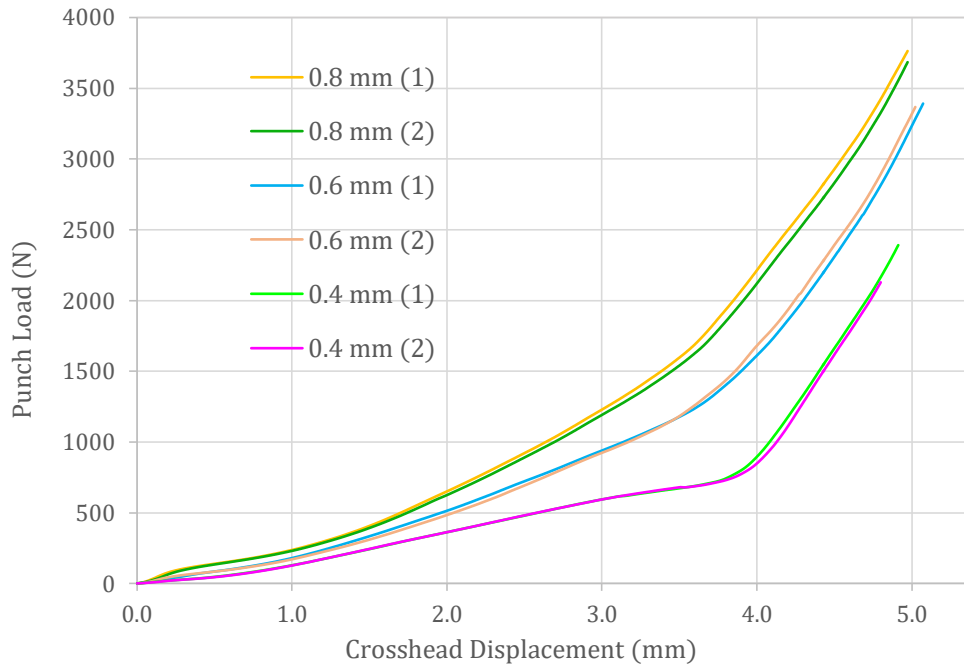


Figure 4.3.1: Punch load versus crosshead displacement plots for aluminum 3003-H14 blank specimens of 0.8 mm, 0.6 mm, and 0.4 mm thicknesses

The load versus displacement plots for two sets of both copper specimen thicknesses are shown in figure 4.3.2; the results for each thickness were consistent with expectations, but the 0.2 mm specimen showed some unique behavior, which is most likely explained by the sheet thickness approaching a limit where grain size had a more prevalent effect.

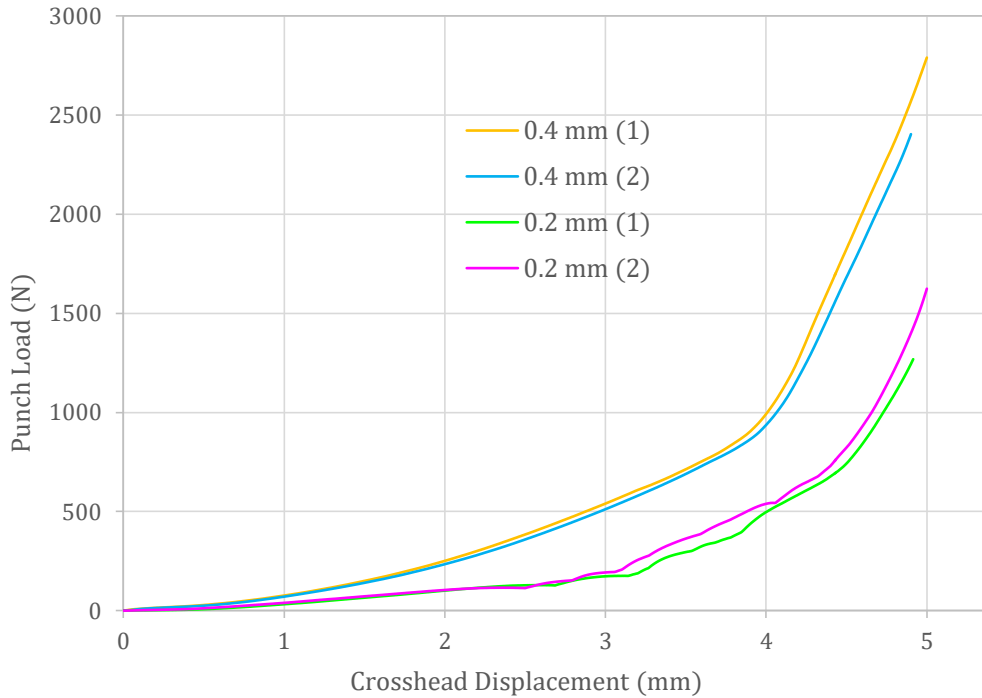


Figure 4.3.2: Punch load versus crosshead displacement plots for 99.9% copper blank specimens of 0.4 mm and 0.2 mm

The copper specimen plots followed many of the same trends that were shown in the aluminum results. The 0.4 mm copper results were similar to the aluminum results for similar thicknesses, which was expected. The 0.2 mm copper plots showed some unique behavior, which was not present for other specimens; these results were divided into three regions (as opposed to two). The first region of primarily bending ended at approximately 2.5 mm of crosshead displacement, at which point a region of irregular portions of constant punch load occurred. This severe plastic strain may be caused by grain size effects, which become more prevalent at smaller thicknesses. The third portion of the plot was similar to the plots from the other specimens.

The final formed shapes for each thickness of the aluminum specimens are shown in figure 4.3.3. There was an obvious crinkle pattern that diminished as the thickness of the specimen increased, and was not obvious in the 0.8 mm specimen. The crinkle pattern was irregular, in that it didn't exhibit symmetry with respect to the amplitude of the crinkle deformation, or the frequency of the crinkles. The irregularity of the pattern may be caused by the anisotropy of the material; because Al 3003-H14 is a cold rolled alloy, there are longer grains in the longitudinal direction of the rolled sheets, which creates slightly different mechanical properties between the longitudinal and transverse directions of the sheet.

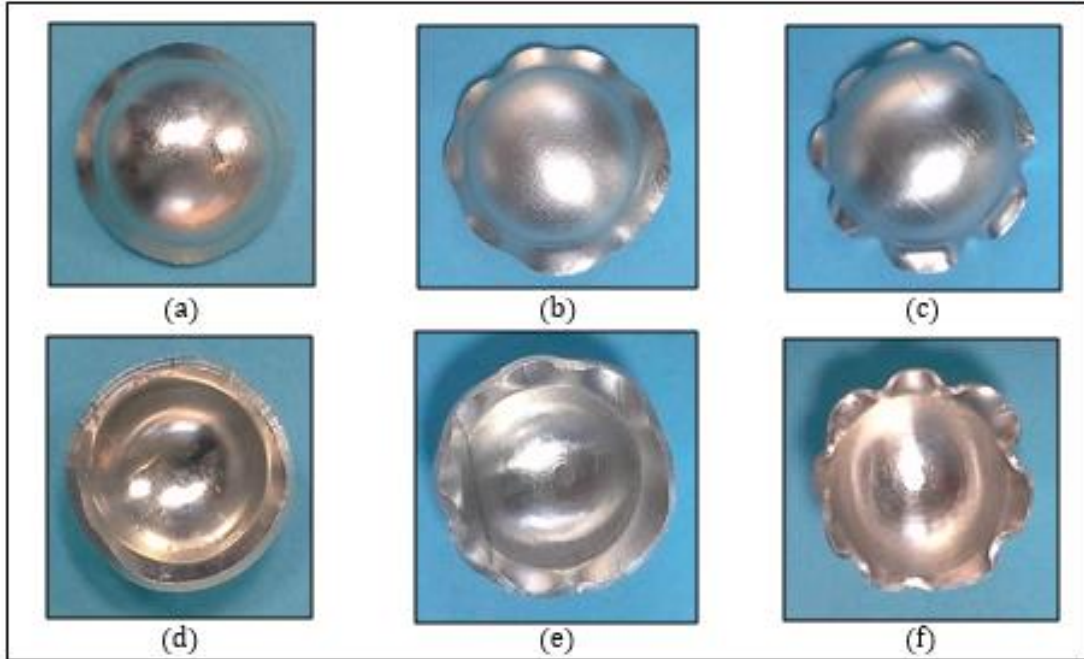


Figure 4.3.3: Final formed shapes of the die side for (a) 0.8 mm aluminum experiment, (b) 0.6 mm aluminum experiment, (c) 0.4 mm aluminum experiment, and the punch side for (d) 0.8 mm aluminum experiment, (e) 0.6 mm aluminum experiment, and (f) 0.4 mm aluminum experiment

The final formed shapes for both thicknesses of the copper specimens are shown in figure 4.3.4. Similar to the aluminum, there were more crinkles as the sheet thickness decreased, and the degree of plastic deformation was greater.

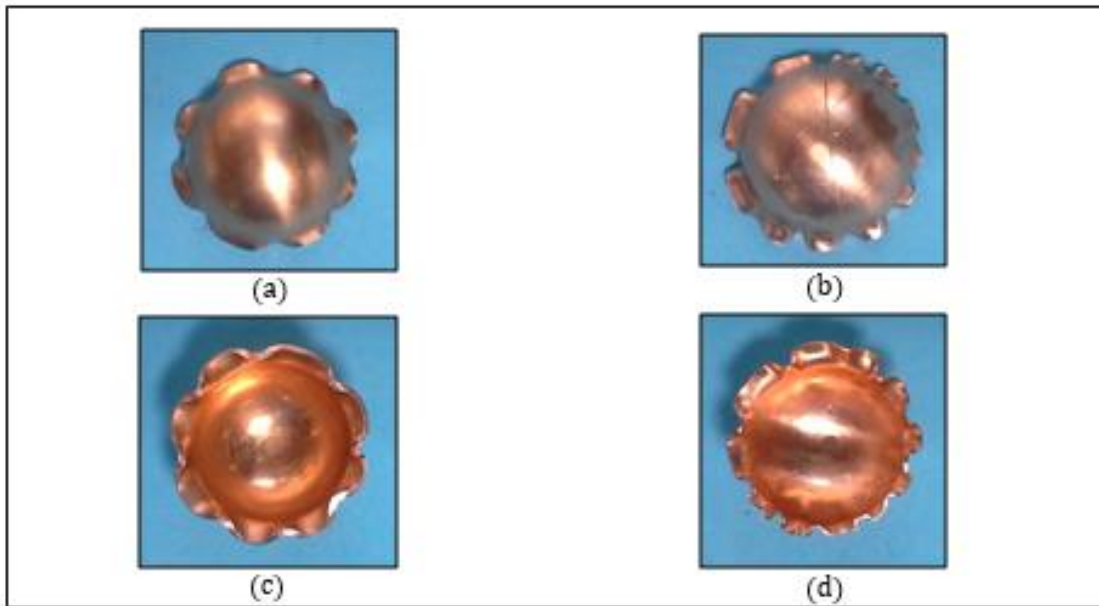


Figure 4.3.4: Final formed shapes of the die side for (a) 0.4 mm copper experiment, (b) 0.2 mm copper experiment, and the punch side for (c) 0.4 mm copper experiment, and (d) 0.2 mm copper experiment

The patterns of crinkles were irregular in both specimens, similar to the aluminum samples. It is unknown whether the copper sheets were work hardened, and therefore have anisotropic material properties.

4.4: Simulation Forming Test Results

The load versus displacement plots for each thickness of aluminum and copper were plotted with the respective experimental results for comparison. Images of the final form geometry were captured for each specification, and compared to the final form of the experimental specimen. Additionally, the final cross sectional thickness was measured, and these results were plotted as thickness versus radius.

Comparisons of the experimental and simulation load versus displacement plots for the forming tests are shown in figure 4.4.1; there was consistency for the results of each thickness. The 0.4 mm thickness simulation plot shows the same distinct change in slope at approximately 3.8 mm displacement. As the thickness increased, the transition became less prevalent, and the 0.8 mm plot shows an exponential increase with a minimal transition at 3.5 mm. There was one portion of the plot that showed inconsistency between the compared plots. Each simulation diverges from the experimental plots at the 4.5–4.8 mm, where the simulated slopes increased greatly; the degree of divergence at this portion of the plot increased as the thickness of the specimen increased. The experimental plots did not diverge from the respective trends at that portion. The Mises stresses and equivalent plastic strain contours for each aluminum specimen are shown in figures A.7-A.9.

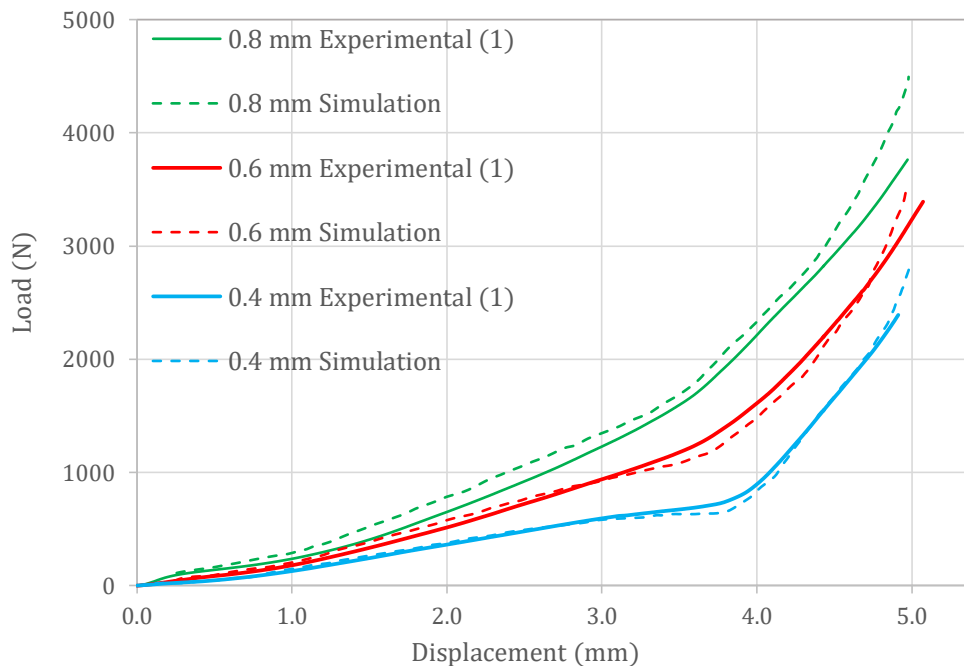


Figure 4.4.1: Comparison of experimental and numerical plots of punch load versus crosshead displacement results obtained for aluminum 3003-H14 blank specimens of 0.8 mm, 0.6 mm, and 0.4 mm

Figure 4.4.2 shows the load versus displacement plot comparison of the experimental and simulation results for both thicknesses of copper. Similar to the aluminum plot comparison, there was good agreement between the simulation and experimental plots for each thickness of copper. The Mises stresses and equivalent plastic strain contours for the 0.2 mm and 0.4 mm copper simulations are shown in figures A.10 and A.11, respectively.

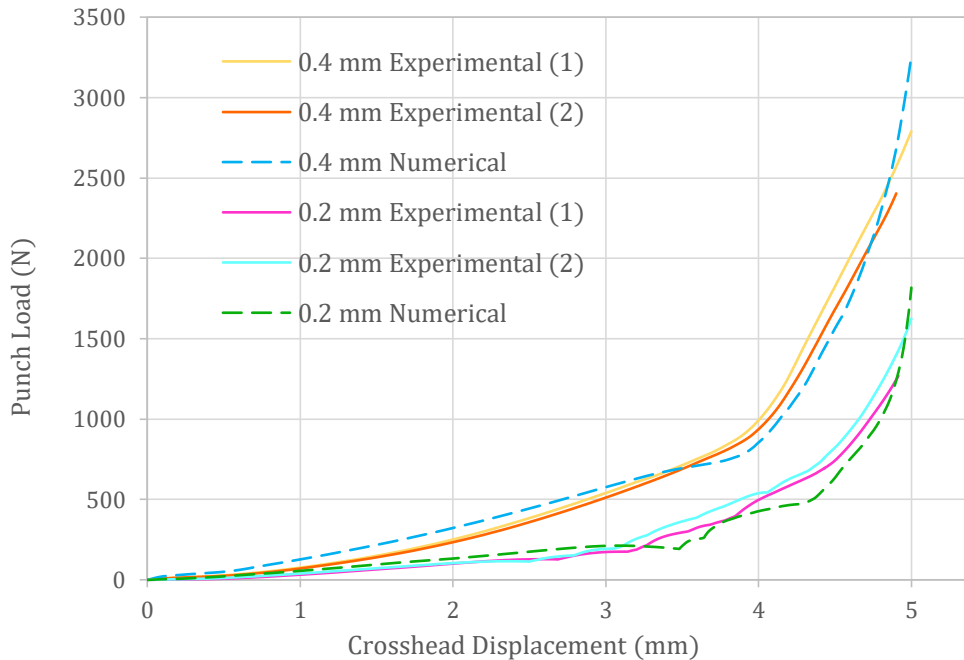


Figure 4.4.2: Comparison of experimental and numerical plots of punch load versus crosshead displacement results obtained for 99.9% copper blank specimens of 0.4 mm and 0.2 mm

The simulation of the 0.2 mm copper thickness showed the same irregular behavior that was present in the experiment. This may be explained by sliding at the blank and punch/die interfaces, when there was less surface contact; as the blank deformed around the punch, the membrane response became prevalent, and the load increased steadily through the remaining portion of the process. The 0.4 mm plots were similar to the aluminum plots, in that there were two distinct linear regions throughout the process. The last portion (approximately 4.5-4.6 mm displacement) of the simulation plot also had the similar divergence from the trend from a linear to an exponential increase in punch load; the 0.2 mm showed the divergence to a lesser degree. It is possible that the simulation inputs for the resin material properties could be improved by introducing a secant and tangent modulus.

Figure 4.4.3 shows a comparison of the experimental and simulation final geometries for each thickness of both materials. There was mostly good agreement between the two methods, but the simulations show an idealized symmetrical pattern, which was expected due to the symmetry boundary conditions and isotropic material properties. This deviation could possibly be resolved by modeling the workpiece with no symmetry conditions and anisotropic material properties, which is discussed further in Chapter 5.

The increasing number of crinkles can be understood by considering the stresses at various points in the forming process. As the tip of the punch first makes contact with the specimen, the simply supported blank undergoes bending along each radius. As the punch displacement increases, the bending occurs across chords of decreasing length, moving outward from the center to the edge; the bending along these chords produced circumferential hoop stresses, which created buckling in the edges if the thickness of the specimen was not sufficient to resist the stresses.

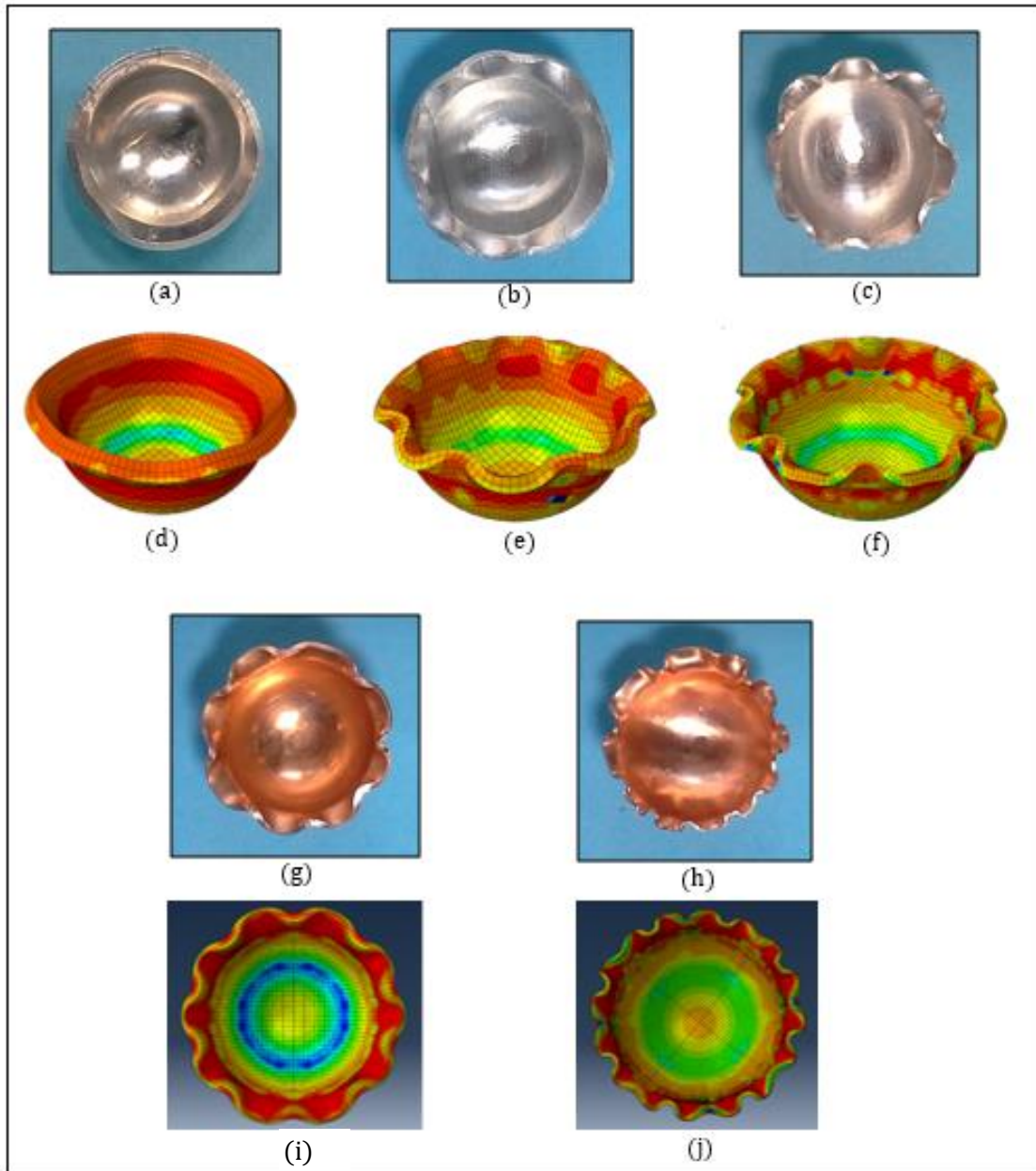


Figure 4.4.3: Final formed shapes of (a) 0.8 mm aluminum experiment, (b) 0.6 mm aluminum experiment, (c) 0.4 mm aluminum experiment, (d) 0.8 mm aluminum simulation, (e) 0.6 mm aluminum simulation, (f) 0.4 mm aluminum simulation, (g) 0.2 mm copper experiment, (h) 0.4 mm copper experiment, (i) 0.2 mm copper simulation, and (j) 0.4 mm copper simulation

4.5: Cross-sectional Thickness:

The cross-sectional thickness of the final forms were obtained for both thicknesses of the copper simulation, and the 0.4 mm copper experiment; the plots of thickness as a function of radius are shown and figure 4.5.1, and the thickness and radius values are shown in table 4.5.1.

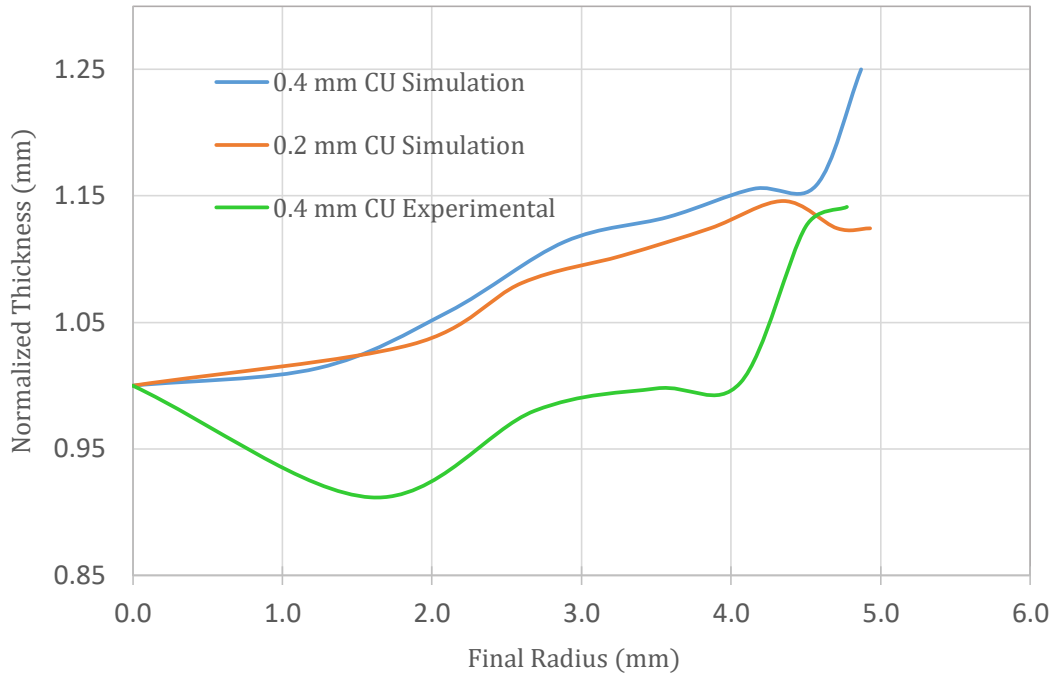


Figure 4.5.1: Comparison of normalized thickness vs final radius plots for the 0.4 mm copper experiment, the 0.2 mm copper simulation, and 0.4 mm copper simulation

The thickness of the specimen decreased as the radius decreased for both specimens; the only exception was for the first few data points of the 0.2 mm specimen, the radius increased. This was most likely a result of the specific geometry of the crinkle on that cross-sectional axis. The 0.4 mm specimen showed a sharp decrease in the thickness at the same range of radial distance. The thickness measurements of the experimental 0.4 mm copper specimen were not in agreement with the simulation or expectations. There is a portion where the experimental form increased from 1.5 mm to the center of the bowl. This may be caused by error from the angle of the cutting plane at that portion of the bowl; if the specimen was cut at an angle, the thickness would be altered at some points but not throughout the entire thickness. This angle would have to be significant to cause a significant measurable error, so this is likely not the only source of error for this measurement.

Table 4.5.1: Results of normalized thickness vs final radius plots for the 0.4 mm copper experiment, the 0.2 mm copper simulation, and 0.4 mm copper simulation

0.2 mm Copper Simulation		0.4 mm Copper Simulation		0.4 mm Copper Experiment	
Final Radius (mm)	Thickness (mm)	Final Radius (mm)	Thickness (mm)	Final Radius (mm)	Thickness (mm)
0	0.873	0	0.800	0	0.876
1.86	0.901	1.24	0.811	1.59	0.799
2.6	0.943	2.11	0.847	2.69	0.859
3.27	0.962	2.89	0.891	3.50	0.874
3.86	0.981	3.58	0.907	4.06	0.878
4.35	1.00	4.15	0.924	4.50	0.987
4.71	0.981	4.57	0.927	4.78	1.00
4.93	0.981	4.87	1.00		

Figure 4.5.2 shows the images of the simulated form for both copper specimen thicknesses. It is obvious that the cross-section does not occur at the same location in the crinkle pattern for the two specimens. This is partially caused by the dissimilarity between the crinkle patterns; the 0.2 mm specimen cross-section occurs in a location that did not exist for the 0.4 mm form, due to the specific crinkle geometry of the thinner form.

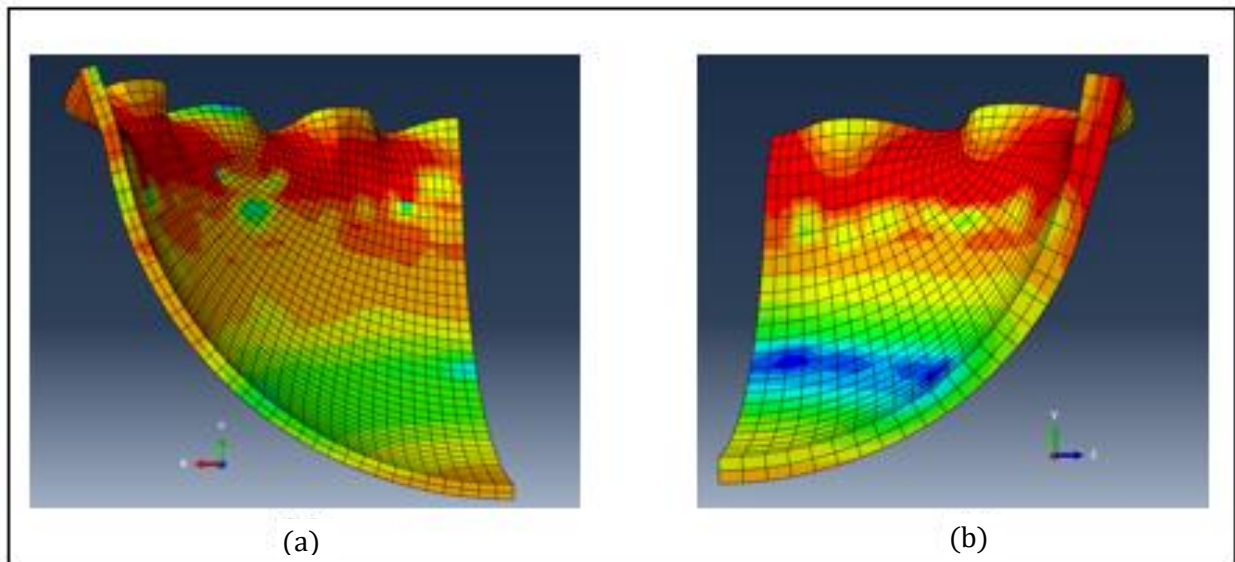


Figure 4.5.2: Cross sectional wedges displaying the thickness through the (a) 0.2 mm and (b) 0.4 mm simulated copper forms

Figure 4.4.6 shows images of the 0.4 mm cross-section, which was mounted and cut from a formed specimen. The method of obtaining the final radius at locations of thickness measurements is shown in these images. An enlarged composite mosaic of the image used to determine the final radius can be seen in figure A.12, and all of the macrographs at the various intersections are shown in figure A.13.

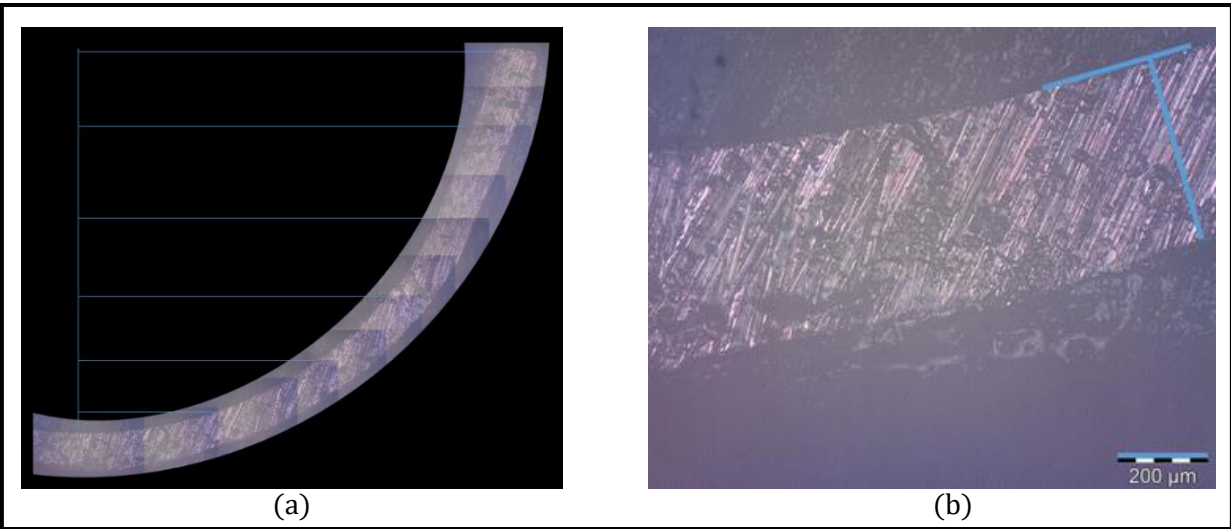


Figure 4.4.6: Cross-sectional macrographs of the 0.4 mm copper formed specimen, (a) as a mosaic of the entire cross-section, pieced together from twelve images to measure the final radius, and (b) an individual macrograph, displaying the method used to measure the thickness

The thickness measurements of the experimental 0.4 mm copper specimen were not in agreement with expectations; the final thickness was greater than the initial thickness of the sheet throughout the entire formed specimen. This may have been caused by the calibration of the scale bar on the microscope; this issue is discussed further in the recommendations section 5.2.

Chapter 5: Conclusions and Recommendations

5.1: Conclusions

The results demonstrated that SLA printed parts could be used in a small-scale forming process, with an accurate simulation prediction. There was good agreement between the experimental and numerical methods for the final load/displacement results, and specific aspects of the final geometries. The demonstrated method can be used to test a wide combination of form shapes, as well as alternate sizes and clearances of similar shapes.

The load versus displacement plots showed agreement between the initial bending stresses and the onset of the circumferential hoop stresses at approximately 75-80 % of the total crosshead displacement (depth of die). The displacement value of the hoop stress onset decreased with and increased specimen thickness. This was most likely caused by increased interference between the punch and die clearance around the brim.

The geometry of the final formed shapes also showed good agreement between the two methods, though there were some inconsistencies in this area. The crinkle pattern behavior was represented in both methods, in that the size and pattern changed to the same degree within each method. The irregular pattern that was demonstrated in the experiment was not reflected in the simulation. This may be resolved by remodeling the workpiece with anisotropic material properties, as opposed to isotropic properties.

There was not as close agreement between the results of the thickness measurements and simulated thickness predictions. There were not only deviations between the copper experimental and simulation results, but also between simulations of the two different thicknesses. The inconsistencies between the experimental and simulation results were significant, and should be further investigated to determine if the variation was caused by error; the deviations between the two simulations were mostly insignificant and were not the result of an error.

5.2: Recommendations

There are several areas of this study which can be improved upon, and other areas which can be built upon, for both the experiment and simulation. The experimental method could be improved by using alternate equipment and specimen preparation methods. The simulation could be improved by using more accurate material characterization inputs.

The tensile tests for each material could be improved by using an extensometer; the UTM crosshead displacement data is not the most accurate method of obtaining the change in gage length. Many of the tensile results showed an initial slip in the crosshead displacement, and there was a degree of interpretation used to determine the modulus slope and plastic curve. An extensometer would allow a more accurate method for comparison.

An alternate machining process could be used, to achieve more optimal surface finishes and tolerances. The CNC machining process will likely leave residual stresses along the cut edges of the specimens. The effects of these stresses would likely become more significant as the specimen thickness decreases.

The method of preparing the formed specimens for thickness measurements should be revised by using an alternative mounting material and cutting method. The accuracy of the cut angle, and path could be improved by using an automated cutting process.

The simulation could be improved by modeling the material as anisotropic, as opposed to isotropic. This could resolve the inconsistencies in the final form geometric predictions, with respect to crinkle symmetry and thickness measurements.

The study could be advanced by conducting the same investigation of the same materials, after they have been annealed. The annealed specimens could be tested using the same hemispherical geometry. This would provide more insight into the degree that grain and geometric size affects the results. This would also give further insight into the effect of the strain hardening on the aluminum specimens. This analysis would require a metallographic analysis comparison of both the strain hardened and annealed specimens.

References

- [1] Steinhauser, M. O., & Hiermaier, S. (2009, December 1). A Review of Computational Methods in Materials Science: Examples from Shock-Wave and Polymer Physics. *International Journal of Molecular Sciences*, 10(12), 5135-5216. doi:doi: 10.3390/ijms10125135
- [2] Callister, William D. Jr., Rethwisch, David G. (2010). *Material Science and Engineering: an Introduction*. 8th edition. Hoboken. John Wiley and Sons, Inc.
- [3] Huerta, E., Corona, J. E., Oliva, A. I., Aviles, F., & Gonzalez-Hernandez, J. (2010, August). Universal testing machine for mechanical properties of thin metals. *Revista Mexicana de Fisica*, 4(56), 317-322.
- [4] Walker, J. R. (2000). *Machining Fundamentals: From Basic to Advanced Techniques*. Tinley Park: The Goodheart-Willcox Company, Inc.
- [5] Gong, F., & Guo, B. (2014). Size Effects on Mechanical Properties of Copper Thin Sheet in Uniaxial Tests. *Material Science (Medziagotyra)*, 20(4), 509-512.
- [6] Chang, T. A., Razali, A. R., Zainudun, N. A., & Yap, W. L. (2015). Size effects in thin sheet metal forming. *IOP Conference Series: Materials Science and Engineering* (pp. 1-10). IOP Publishing.
- [7] Anand, D., & Kavi, D. R. (2014). Effect of thickness and grain size on flow stress of very thin brass sheets. *Procedia Materials Science*, 154-156.
- [8] Jiang, Z., Zhao, J., & Xie, H. (2017). *Microforming Technology: Theory, Simulation, and Practice*. London: Academic Press.
- [9] Jameson, E. C. (2001). *Electric Discharge Machining*. Dearborn: Society of Manufacturing Engineers.
- [10] Arif, M., & Rahman, M. (2014). Fundamentals and Modeling of Micro-End Milling. *Comprehensive Materials Processing*, 11, 179-199.
- [11] Rane, A. V., Kanny, K., & Thomas, S. (2018). *Synthesis of Inorganic Nanomaterials*. Cambridge, MA: Woodhead Publishing; Elsevier.
- [12] Mu, Y., Hutchinson, J., & Meng, W. (2014). Micro-pillar measurements of plasticity in confined Cu thin films. *Extreme Mechanics Letters*, 62-69.
- [13] Zguris, Z. (n.d.). *How Mechanical Properties of Stereolithography 3D Prints are Affected by UV Curing*. Formlabs.
- [14] Black, J., & Kohser, R. A. (2013). *DeGarmo's Material and Processes in Manufacturing*. Hoboken: John Wiley and Sons, Inc.

- [15] Pearce, R. (1991). *The Adam Hilger Series on New Manufacturing Processes and Materials*. Philadelphia: IOP.
- [16] Pantano, M. F., Espinosa, H. D., & Pagnotta, L. (2011). Mechanical characterization of materials at small scale lengths. *Journal of Mechanical Science and Technology*, 26(2), 545-561.
- [17] Raulea, L. V., Goijaerts, L., Govaert, L. E., & Baaijens, F. (2001). Size effects in the processing of thin metal sheets. *Journal of Material Processing Technology*, 115, 44-48.
- [18] Chan, W. L., Fu, M., & Yang, B. (2011). Study of size effect in micro-extrusion process of pure copper. *Material and Design*, 32, 3772-3782.
- [19] Senthil Kumar, V. S., Viswanathan, D., & Natarajan, S. (2006). Theoretical prediction and FEM analysis of superplastic forming of AA7475 aluminum alloy in a hemispherical die. *Journal of Materials Processing and Technology*, 173, 247-251.
- [20] Wang, X., & Cao, J. (2000). On the prediction of side-wall wrinkling in sheet metal forming processes. *International Journal of Mechanical Sciences*, 42, 2369-2394.
- [21] Kim, H., & Kardes, N. (2012). *Sheet Metal Forming: Fundamentals*. Materials Park: ASM International.
- [22] Olsson, D., Bay, N., & Andreasen, J. O. (2010). A quantitative lubricant test for deep drawing. *International Journal of Surface Science and Engineering*, 4(1), 1-12.
- [23] Folle, L. F., & Schaeffer, L. (2019). Effect of surface roughness and lubrication on the friction coefficient in deep drawing processes of aluminum alloy AA1100 with fem analysis. *Materia (Rio de Janeiro)*, 24(1). doi:<http://dx.doi.org/10.1590/s1517-707620190001.0635>
- [24] Cao, J., Krishnan, N., Wang, Z., Lu, H., Liu, W., & Swanson, A. (2004, November). Microforming: Experimental Investigation of the Extrusion Process for Micropins and its Numerical Simulation Using RKEM. *ASME*, 126, 642-652.
- [25] Qin, Y., Brockett, A., Ma, Y., Razali, A., Zhao, J., Harrison, C., . . . Loziak, D. (2010). Micro-manufacturing: research, technology outcomes and development issues. *International Journal of Advanced Manufacturing Technology*, 47, 821-837.
- [26] Razali, A. R., & Qin, Y. (2013). A Review on Micro-manufacturing, Micro-forming and their Key Issues. *Procedia Engineering*, 53, 665-672.
- [27] Liu, J. G., Fu, M., Lu, J., & Chan, W. L. (2011). Influence of size effect on the springback of sheet metal foils in micro-bending. *Computational Material Science*, 50, 2604-2614.
- [28] Fulop, T., Brekelmans, W., & Geers, M. (2006). Size effects from grain statistics in ultra-thin metal sheets. *Journal of Materials Processing Technology*, 174, 233-238.
- [29] Engel, U. (2006, February 10). Tribology in microforming. *Wear*, 260 (3), 265-273.

- [30] Geiger, M.; Geibdorfer, S.; Engel, U.: Mesoscopic model - advanced simulation of micro-forming Processes, Cardiff, U.K. Whittles Publishing, Ltd.
- [31] Sanusi, K. O., & Oosthuizen, G. A. (2011). Finite Element Modelling of the Effects of Average Grain Size and Misorientation Angle on the Deformation. *International Journal of Multiphysics*, 5(3), 275-286.
- [32] Kim, G.-Y., & Ni, J. (2007, June). Modeling of the Size Effects on the Behavior of Metals in Microscale Deformation Processes. *ASME*, 129, 470-476.
- [33] Atlas Steels, "Aluminum Alloy Datasheet: 3003," October 2013
- [34] Copper Development Association Inc., "Application Data Sheet: Mechanical Properties of Copper and Copper Alloys at Low Temperatures," 144/8.

Appendix

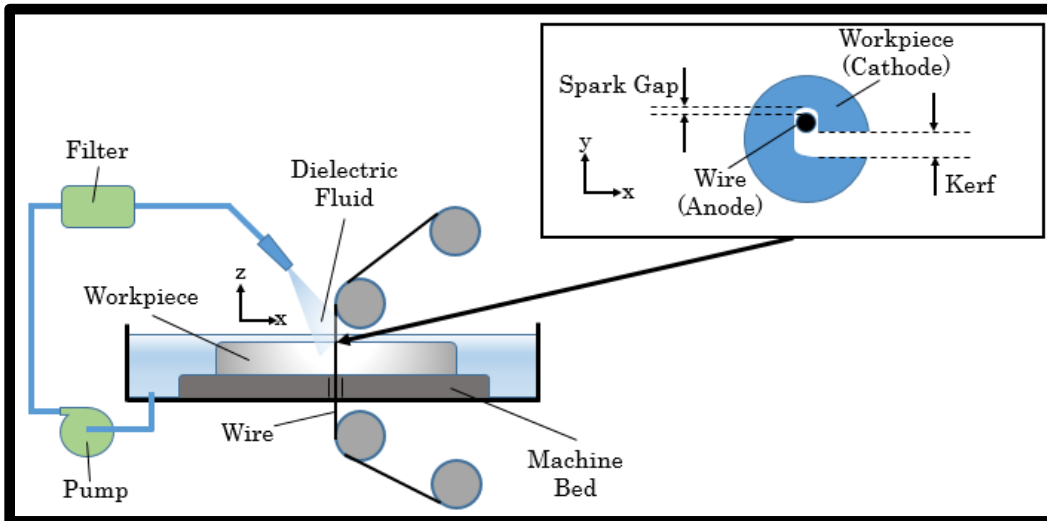


Figure A.1: Diagram showing a wire-cutting EDM process

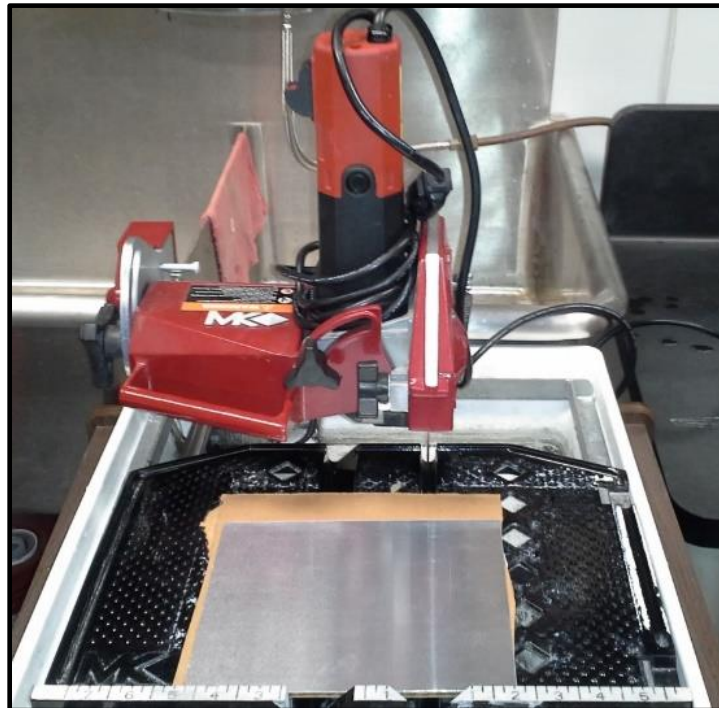


Figure A.2: MK diamond wet saw, and sectioning setup

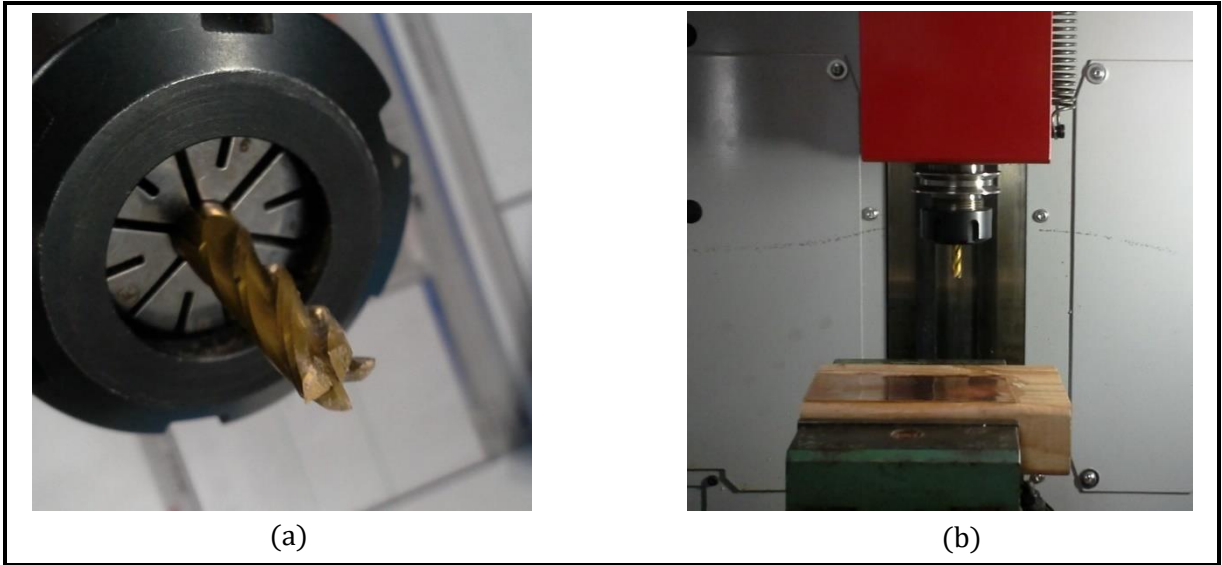


Figure A.3: Images of: (a) the end-mill mounted in the collet, and (b) the CNC machining setup

Table A.1: Strain gauge specifications, testing parameters, and tensile specimen dimensions

Grid Resistance	Gage Factor	Ambient Temperature	Voltage	Thickness (mm)	Width (mm)
350.0 Ω	2.150	23 °C	3.5 mV/V	0.780	9.95

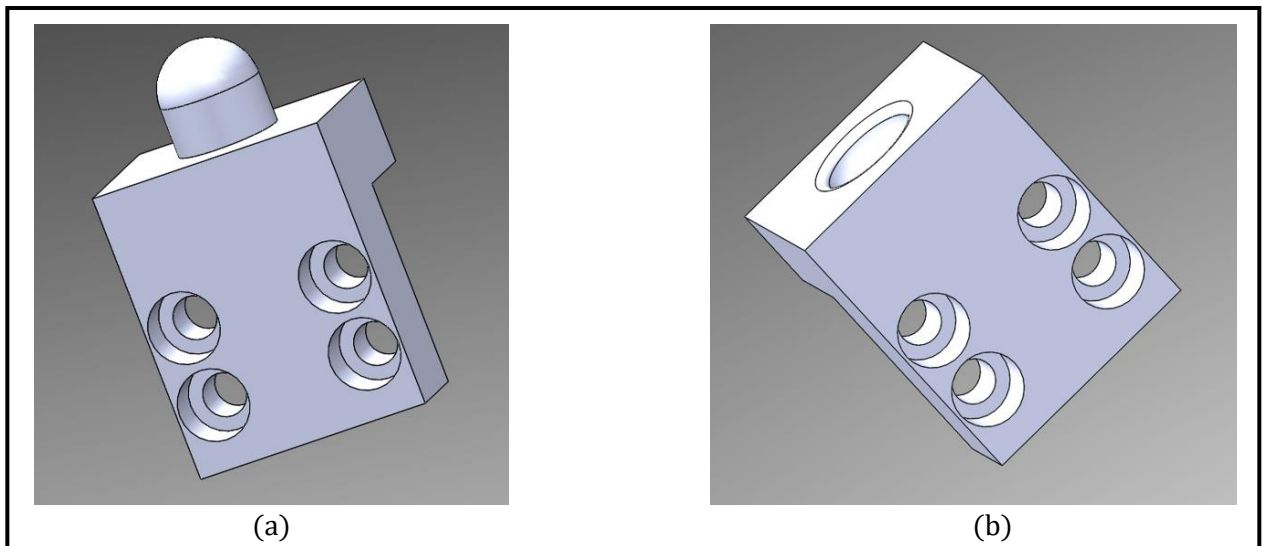


Figure A.4: SolidWorks model of the hemispherical (a) punch and (b) die

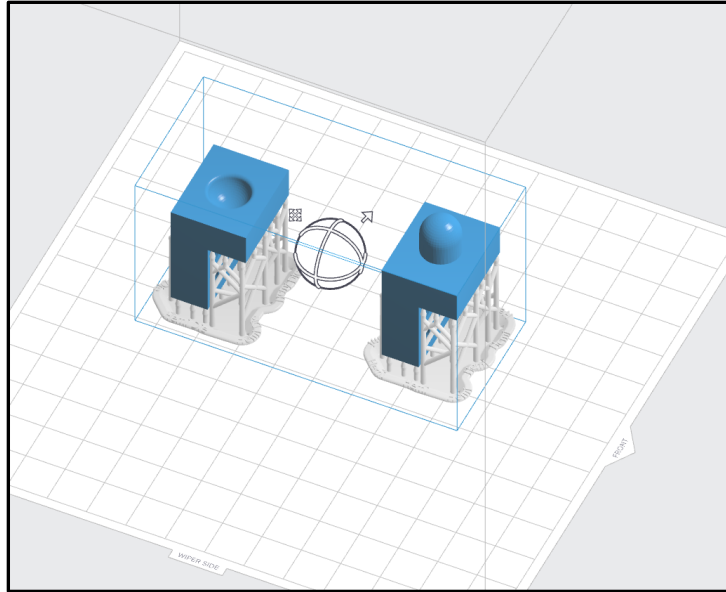


Figure A.5: 3d-printing setup for the hemispherical punch and die in PreForm slicer software

Table A.2: Tensile properties of Aluminm 3003-H14 for varying ranges of sheet thickness [33]

Material	Modulus of Elasticity (GPa)	Yield Strength (MPa)	Ultimate Strength (MPa)	Elongation (%)		
				0.20-0.32 (mm)	0.33-0.63 (mm)	0.64-1.20 (mm)
AL 3003-H14	69.0	115	140-180	1.0	2.0	3.0

Table A.3: Tensile properties of 99.9% copper [34]

Material	Modulus of Elasticity (GPa)	Yield Strength (MPa)	Ultimate Strength (MPa)	Elongation (%)
CU - 99.9 %	110-120	82-110	180-250	0.4-0.6

Table A.4: Measured cross sectional geometry (thickness and width) of the dog-bone tensile specimens for each material

Aluminum		Copper		Resin	
Thickness (mm)	Width (mm)	Thickness (mm)	Width (mm)	Thickness (mm)	Width (mm)
0.791	5.91	0.412	5.87	1.95	4.49
0.787	5.90	0.226	5.90	1.98	4.47
0.789	4.95			1.95	4.45
0.621	5.97			1.98	4.50
0.617	5.95			1.94	4.45
0.620	4.96				
0.414	5.02				
0.416	4.98				
0.420	5.02				

Table A.5: Plastic flow inputs for the aluminum and copper simulations

Aluminum		Copper	
Strain	Flow Stress (MPa)	Strain	Flow Stress (MPa)
0.000	145	0.000	90
0.125	155	0.100	140
0.250	163	0.300	165
0.375	168	0.500	170
0.500	173	0.600	171
1.00	178		
2.00	180		

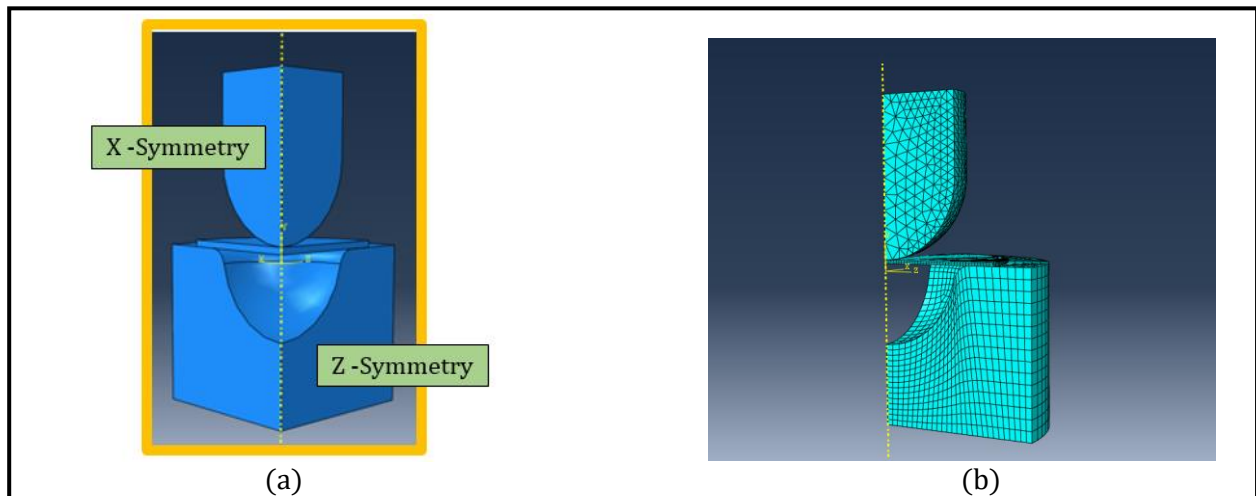


Figure A.6: Images of simulation assembly (a) symmetry conditions and (b) mesh for 0.4 mm copper

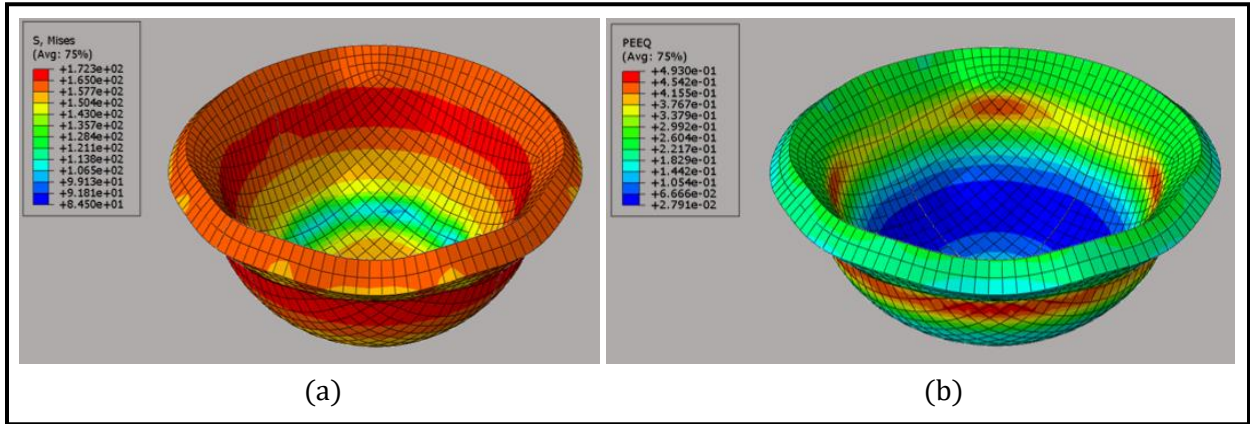


Figure A.7: Contours of (a) Von Mises stresses, and (b) equivalent plastic strain, for the 0.8 mm aluminum forming simulation

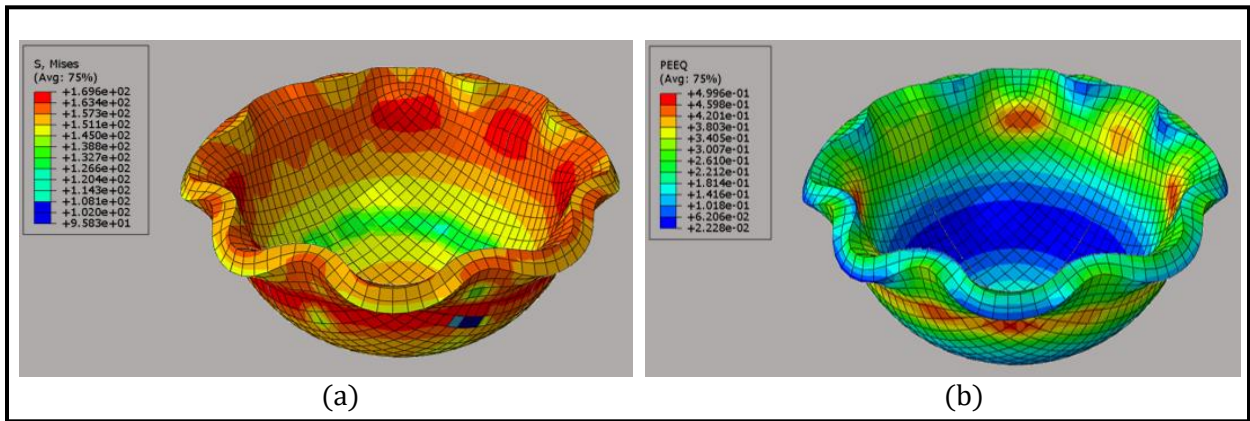


Figure A.8: Contours of (a) Von Mises stresses, and (b) equivalent plastic strain, for the 0.6 mm aluminum forming simulation

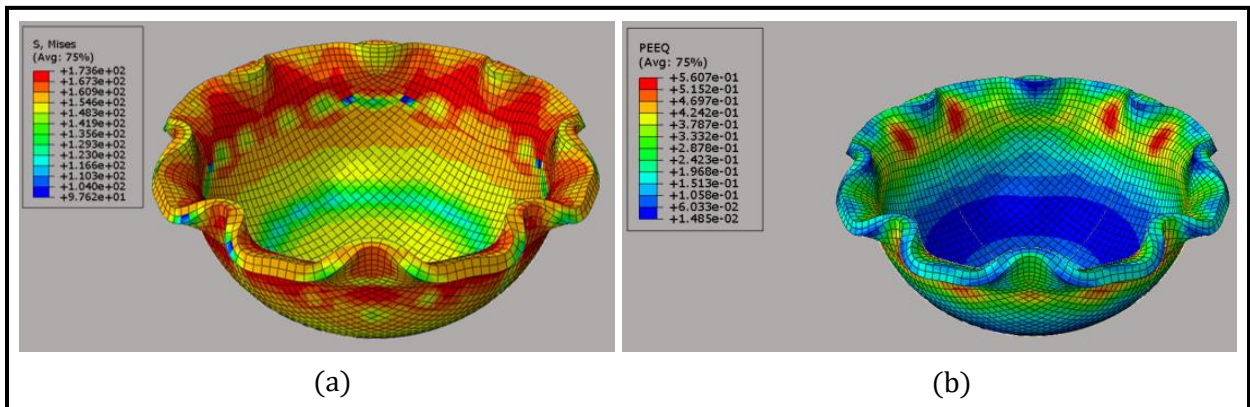


Figure A.9: Contours of (a) Von Mises stresses, and (b) equivalent plastic strain, for the 0.8 mm aluminum forming simulation

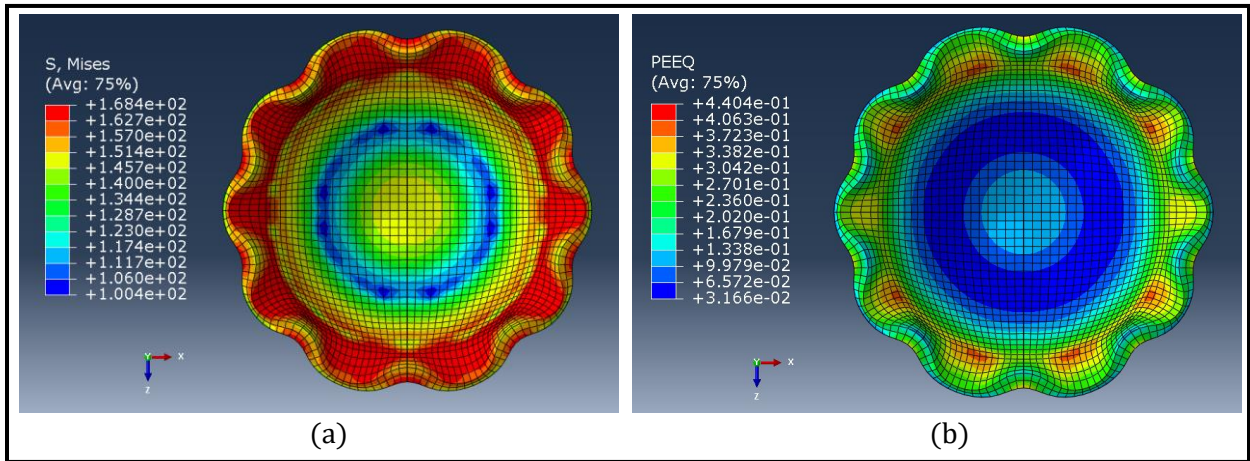


Figure A.10: Contours of (a) Von Mises stresses, and (b) equivalent plastic strain, for the 0.4 mm copper forming simulation

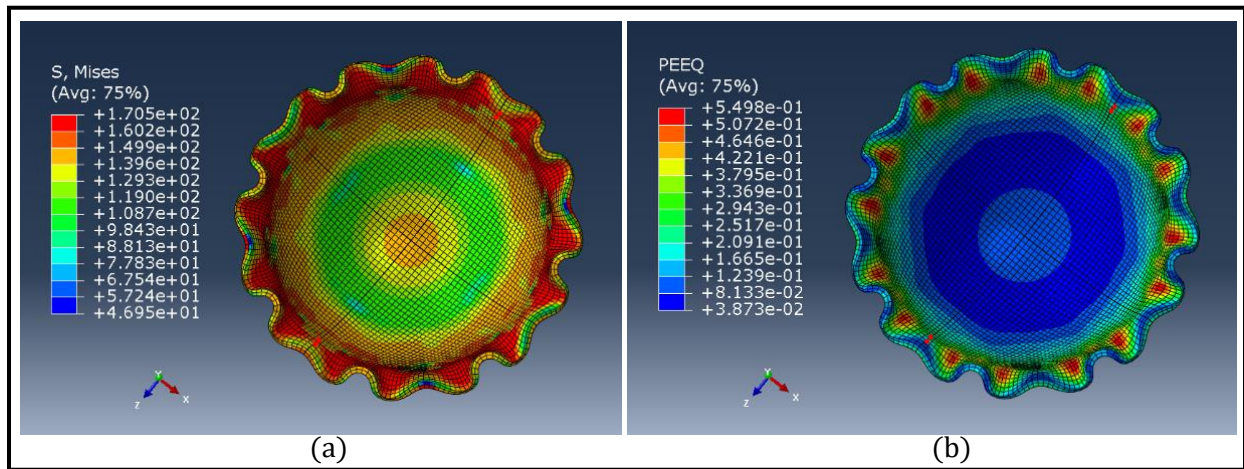


Figure A.11: Contours of (a) Von Mises stresses, and (b) equivalent plastic strain, for the 0.2 mm copper forming simulation

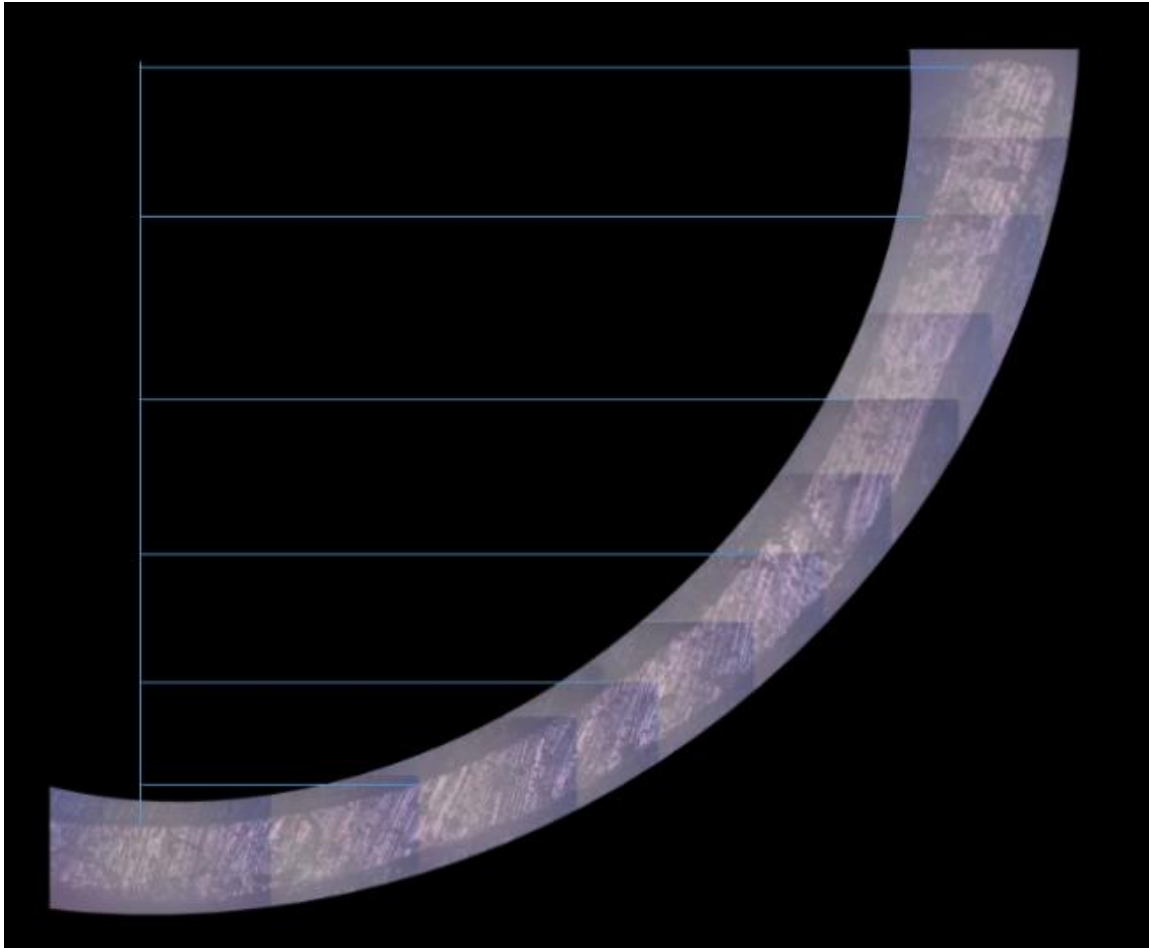


Figure A.12: Macrograph composite of copper 0.4 mm cross-section, showing the method of determining the final formed radius measurements

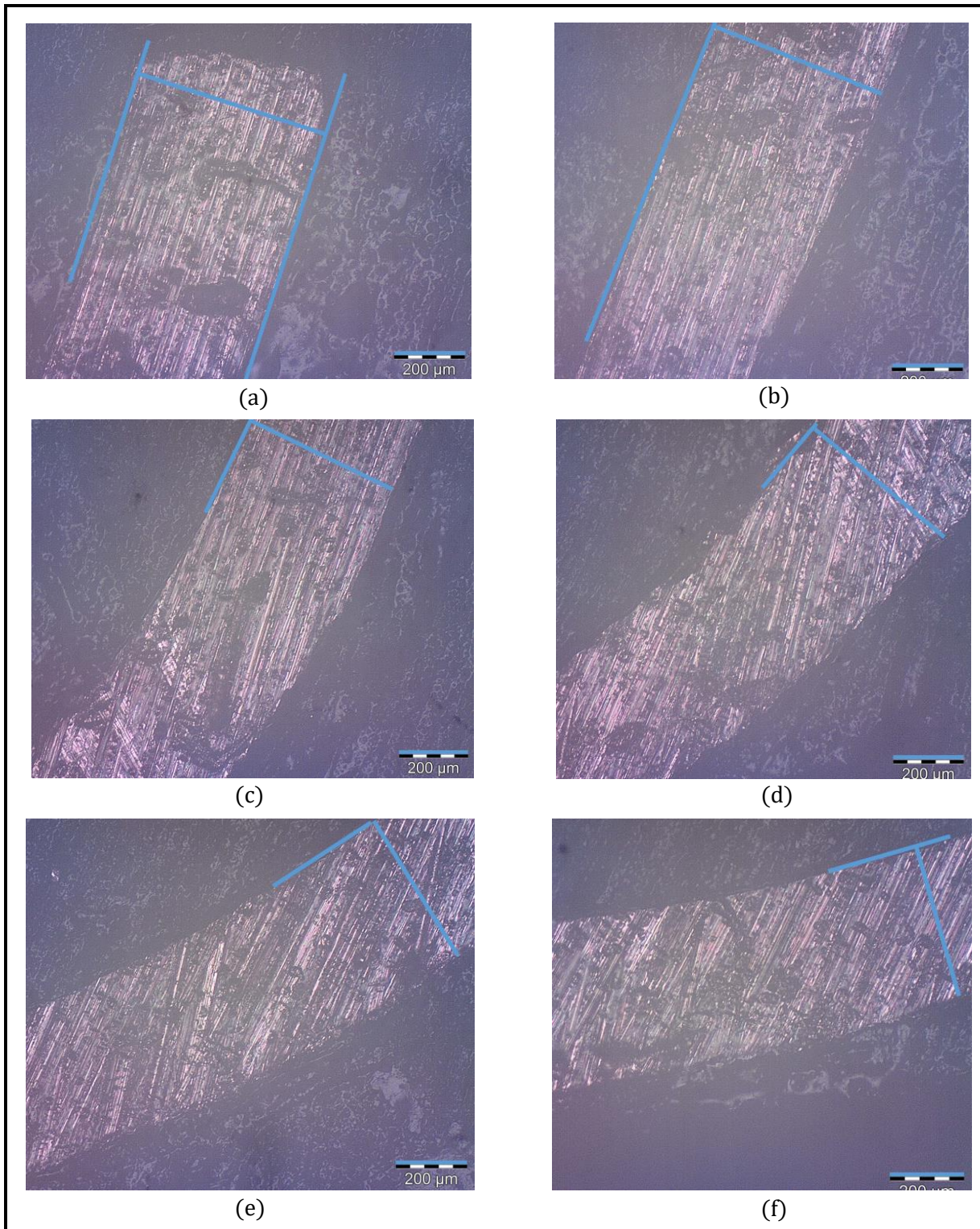


Figure A.13: Macrographs of various cross-sections showing the thickness measurement method at a final radius of: (a) 4.78 mm (b) 4.50 mm (c) 4.06 mm (d) 3.50 mm (e) 2.69 mm (f) 1.59 mm

Vita

The author was born in Metairie, Louisiana. He obtained his Bachelor's degree in mechanical engineering from the University of New Orleans in 2014. He entered the University of New Orleans graduate program to pursue a Master of Science in mechanical engineering in 2017, and joined Professor Paul Schilling's and Professor Paul Herrington's research team.